sensors

MDPI

Review

TiO_2-Based Nanoheterostructures for Promoting Gas Sensitivity Performance: Designs, Developments, and Prospects

Yuan Wang [1,2,*,†], Tao Wu [1,2,†], Yun Zhou [1,3], Chuanmin Meng [1], Wenjun Zhu [1] and Lixin Liu [1,*]

1 National Key Laboratory of Shock Wave and Detonation Physics, Institute of Fluid Physics, China Academy of Engineering Physics, PO Box 919-111, Mianyang 621900, Sichuan, China; tomasiwt@gmail.com (T.W.); zhouyun720@126.com (Y.Z.); mcm901570@126.com (C.M.); wjzhu@caep.ac.cn (W.Z.)

2 School of National Defense Science and Technology, Southwest University for Science and Technology, Mianyang 621900, Sichuan, China

3 School of Materials Science and Engineering, Xiangtan University, Xiangtan 411105, Hunan, China

* Correspondence: wangyuan0000@gmail.com (Y.W.); liulix00@gmail.com (L.L.); Tel.: +86-816-2482239 (Y.W.); +86-816-2491281 (L.L.)

† These authors contributed equally to this work.

Received: 2 July 2017; Accepted: 25 August 2017; Published: 27 August 2017

Abstract: Gas sensors based on titanium dioxide (TiO_2) have attracted much public attention during the past decades due to their excellent potential for applications in environmental pollution remediation, transportation industries, personal safety, biology, and medicine. Numerous efforts have therefore been devoted to improving the sensing performance of TiO_2. In those effects, the construct of nanoheterostructures is a promising tactic in gas sensing modification, which shows superior sensing performance to that of the single component-based sensors. In this review, we briefly summarize and highlight the development of TiO_2-based heterostructure gas sensing materials with diverse models, including semiconductor/semiconductor nanoheterostructures, noble metal/semiconductor nanoheterostructures, carbon-group-materials/semiconductor nanoheterostructures, and organic/inorganic nanoheterostructures, which have been investigated for effective enhancement of gas sensing properties through the increase of sensitivity, selectivity, and stability, decrease of optimal work temperature and response/recovery time, and minimization of detectable levels.

Keywords: TiO_2; nanoheterostructures; gas sensor

1. Introduction

Since the 20th century, atmospheric pollution has been proved to be one of most urgent issues. For the sake of controlling the exhaust emissions, gas sensors for the quantitative detection of various toxic and harmful gases have been widely developed as a result of their high response, outstanding selectivity, excellent repeatability, and good stability [1–3]. So far a variety of gas sensors, such as metal oxide semiconductor-based gas sensors [4–9], solid electrolyte-based gas sensors [10], electrochemical gas sensors [11], carbon-based gas sensors [1,12–14], organic gas sensors [2,3], and so on, have been extensively investigated. Amongst these different types of gas sensors, resistance type metal oxide gas sensors offering low cost, simple manufacturing approaches, and excellent sensitivity to the great majority of gases, have attracted considerable attention during the past several years [15,16]. Since Seiyama [17] reported metal oxide-based gas sensors for the first time, a large amount of effort has been expended in exploring the sensing properties of metal oxide- based gas sensors [7,18,19].

As a representative semiconductor metal oxide, titanium dioxide (TiO_2) has attracted much attention since Fujishima et al. observed the photocatalytic splitting of water on a TiO_2 electrode

under the irradiation of UV light in 1972 [20]. In the past decades, it has been discovered that TiO_2 could be employed in many promising fields including photovoltaics [21], photocatalysis [22,23], sensors, etc. [24–26]. In particular, because of its high stability, harsh environmental tolerance, and environmentally-friendly properties, TiO_2 has been widely investigated and is regarded as one of sensing materials for gas detection with the most potential [27–30].

Naturally, TiO_2 mainly exists in three polymorph forms: rutile phase (tetragonal, P42/mnm) [31], anatase phase (tetragonal, I41/amd), and brookite phase (orthorhombic, pbca) (Figure 1a–c), whose bandgaps are 3.02, 3.2, and 2.96 eV, respectively [32]. Besides the abovementioned three crystal phases, there exists another phase, TiO_2(B) (monoclinic, C2/m). As shown in Figure 1d, TiO_2(B) possesses a layer structure, thus the density is lower and the specific capacity is larger comparing with other phases [33–35]. Among these diverse crystal phases, the most stable bulk phase is rutile, whereas for nanomaterials, anatase and brookite are commonly recognized to be more stable phases because of their relatively lower surface energy than rutile, although this fact is still argued in previous reports [36,37]. In the practical applications, TiO_2 performance is commonly affected by the crystal phases, which can be obtained through controlling the experimental conditions, such as fabrication methods, pH, duration annealing, temperature, and so on. As for the sensing applications, rutile TiO_2 and anatase TiO_2 are the most studied polymorphs.

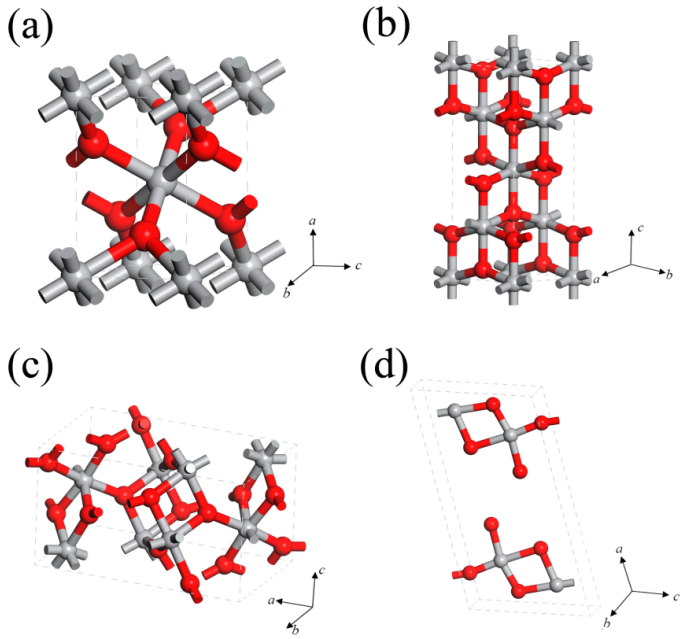

Figure 1. Crystal structures of TiO_2: (**a**) Rutile; (**b**) Anatase; (**c**) Brookite; and (**d**) TiO_2(B), red spheres represent Ti atoms, and the grey spheres represent O atoms.

TiO_2 gas sensors are typical resistant-type sensors which can display a decrease or increase in resistance when probing a reductive gas (H_2, H_2S, NH_3, CO, VOCs) or oxidative gas (NO_2, O_2) [29,30,38], respectively. The sensing mechanism of TiO_2-based gas sensors can be described by the following two-step process: receptor process and transducer process, as shown in Figure 2 [39].

The receptor process occurs at the TiO_2 surface, and it involves physisorption and chemisorption processes [40]. Firstly, oxygen molecules can be physically absorbed on the surface when TiO_2 is exposed to an air environment at room temperature; the process is determined by Van der Waals and dipole interactions; secondly, oxygen molecules on the TiO_2 surface will capture electrons from the conductive band (CB) of TiO_2 to form chemisorbed oxygen species (O_2^-) on the surface. The reactions taking place on the surface of TiO_2 are as follows:

$$O_2(g) \rightarrow O_2(ads) \quad (1)$$

$$O_2(ads) + e \rightarrow O_2^- \quad (2)$$

During the process, receptor capability is determined by the physisorption process and chemisorption process together, where the physisorption can be influenced by the temperature, whereas the rate of chemisorption process may be influenced by activation energy.

The transducer process includes the transportation of electrons in the TiO_2 and the transformation of electrons into the outward resistance signal. This can be influenced by the three typical electron transfer modes which are divided as surface-controlled mode, grain-controlled mode, and neck-controlled mode, respectively, [41,42] as shown in Figure 2. As for surface-controlled mode, compact layer structures determined by the thin film thickness of the materials are universally considered as the main pattern [39], where the gases can only affect the materials surfaces other than the internal body. On the contrary, in real polycrystalline materials, the TiO_2 grains connect to each other through grain boundaries or necks, in this way, the grain boundaries or necks will contribute significantly to the electroconductibility and gas sensing performance of the TiO_2. It has been reported that materials with large grain size would possess large neck cross sections, so accordingly the neck resistance is less significant than the grain-boundary resistance. However, for materials with much smaller grain size, the neck resistance is higher than the grain boundary resistance because of the much smaller neck cross section, in this case the neck resistance becomes more significant [41].

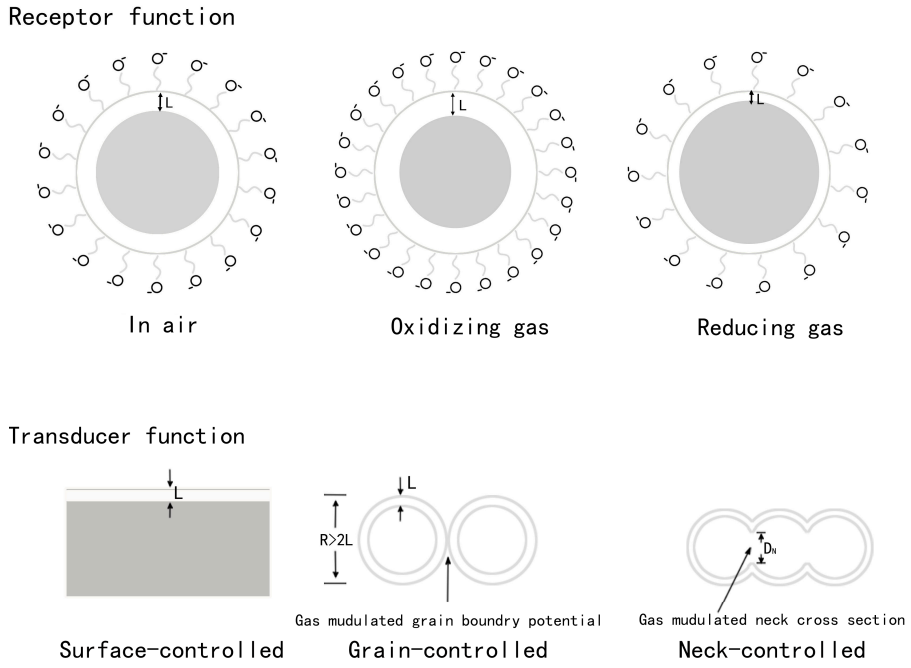

Figure 2. Schematic image of gas sensing at different modes, where L represents the depletion layer, R represents particle size, and D_N represents the diameter of the neck cross section.

In these two typical processes presented above, surface-to-volume ratio, grain size, and the electron transport ability of TiO_2-based materials play important roles. Consequently, in recent years, substantial effort has been invested in increasing the specific surface area, decreasing the grain size, and enhancing the conductivity of TiO_2 through nanostructured materials, element doping, heterostructural materials and so on [27,30,43–46].

Nano-scale is a key factor in studying the gas sensing properties of metal oxide semiconductor-s based sensors. In fact, it is well known that the surface structure and specific surface area can play

very important roles in sensing properties [47]. Nanocrystallization is an efficient way to improve the gas sensing performance because of their much larger specific surface area and rich surface chemical properties on the nanostructure surfaces, which may potentially lead to miniaturized sensors with outstanding performance. In this regard, many kinds of TiO_2 nanostructures with various morphologies, such as zero-dimensional (0D) nanocrystals [48], 1D nanofibers or nanowires [43,49,50], 2D nanoplates [29], and 3D hierarchical microstructures [27] have been developed.

Another important strategy to enhance the sensing performance of TiO_2 is the formation of heterostructures. The heterojunction theory dates back to as early as the 1930s [51]. Since then, more and more applications of nanoheterojunctions have been extensively investigated owning to the superinjection of charge carriers. Since 2005, a great many nanoheterostructural materials have been widely researched and applied in many fields, including solar cells [52], Li-ion batteries [53], photoelectrochemical cells [54], photocatalysis [55], and gas sensors [5,56]. As a matter of fact, several TiO_2-based nanoheterostructures, such as semiconductor/semiconductor, noble metal/ semiconductor, carbon-group-material/semiconductor and organic/inorganic nanoheterostructures, have attracted widespread interest in the preparation and investigation of their properties and applications. Various types of TiO_2-based nanoheterostructures including composite nanoparticles [57–59], quantum dots in nanowires/nanofibers [60–63], core/shell nanowires/nanofibers/ nanospheres [64,65], etc., have been studied intensively. Compared with the pure oxide, these nanoheterostructures achieve higher sensing performance. As a well-known strategy, the modification of TiO_2 nanostructures using noble metal nanoparticles, like platinum (Pt), palladium (Pd), silver (Ag), and gold (Au), forming noble metal/TiO_2 heterostructured sensor materials can further improve the sensing performance, including enhancement of sensitivity and selectivity and shortening of response/recovery times [66,67]. The enhanced properties can be generally ascribed to the catalytic activity of noble metal nanoparticles, increased active surface area, reduced electrical resistance, enhanced optical absorption, facilitated chemical adsorption of oxygen molecules and/or reaction of oxygen ions with probing gases, and improved gas diffusion inside the heterostructures [68]. In addition, the Schottky barrier formed at the interface of noble metal/TiO_2 heterojunction yielding efficient electron/hole separation is considered as another important factor in enhancing sensing performance. In general, the electronic and chemical properties of the metal/oxide interface, as well as the morphology of the noble metal nanoparticles and metal oxides matrix, play important roles in promoting the overall performance of the noble metal/TiO_2 nanoheterostructures [57,60,69,70]. Comprehensive coverage of metal/semiconductor nanoheterostructured sensors have been available elsewhere for many decades, so accordingly, in this review, we briefly trace the application of TiO_2-based semiconductor/semiconductor, carbon-group-material/semiconductor and organic/inorganic nanoheterostructures in the area of gas sensors, summarize their major design and preparation methods, describe some of the improvements and resulting achievements, and discuss the future challenges and perspectives.

2. Fabrication of TiO_2-Based Nanoheterostructures

In the past few decades, various fabrication methods, including chemical vapor deposition (CVD), atomic layer deposition (ALD), solid phase reaction, electrochemical deposition, chemical deposition, hydrothermal/solvothermal methods, sol-gel, electrospinning, etc., have rapidly developed and been successfully applied in preparing high quality TiO_2-based nanoheterostructures. Accordingly, in this section, most of the attention will be focused on the nanoheterostructure synthesis methods.

2.1. CVD and ALD Methods

The CVD route probably is one of most extensively explored approach in nanoheterostructure preparation, which can deposit various materials onto suitable substrates in order. Nanoheterostructures are generally synthesized using a two-step growth procedure. In the first step, the inner-core material is deposited on a suitable substrate through CVD or other synthetic routes. In the second step, the outer-layer shell material is subsequently grown on the core surface.

This method has the capability to control the components, morphology, thickness, and length of the materials by controlling some technological parameters including temperature, pressure, carrier gases, gas-flow rates, substrates, and deposition time. For example, ZnO-TiO_2 nanocomposites were fabricated via an innovative CVD technique [46], where TiO_2 nanoparticles were grown on the initially deposited ZnO nanoplatelet host. The process was carried out at a relatively low temperature of 350–400 °C, this avoiding the effect of unsuitable thermal treatment and maintaining the chemical properties of the materials. Barreca et al. [71] have reported the fabrication of CuO-TiO_2 nanocomposites through a multistep vapor deposition process, where the first step was the synthesis of porous CuO nanomaterials on an Al_2O_3 substrate via a CVD approach, and the final step was the controllable growth of TiO_2 nanoparticles on the porous CuO matrices.

Although involving a similar chemical process as the CVD route, ALD has attracted much attention in the synthesis of heterostructures because of the accurate control of film thickness at atomic scale and the conformal growth of complex nanostructures. The excellent conformability between two materials obtained by ALD makes them possible to form heterojunctions at the semiconductor interfaces. Through growth control, Katoch et al. [72] have successfully prepared TiO_2/ZnO inner/outer double-layer hollow fibers (TiO_2/ZnO DLHFs), as shown in Figure 3. The TiO_2/ZnO DLHFs were synthesized using a three-step process. First, polyvinyl acetate (PVA) fibers were prepared by an electrospinning process; subsequently, TiO_2 and ZnO were sequentially grown on the PVA fibers through the ALD method and, finally, a thermal treatment was carried out for the removal of the PVA support and the crystallization of TiO_2 and ZnO.

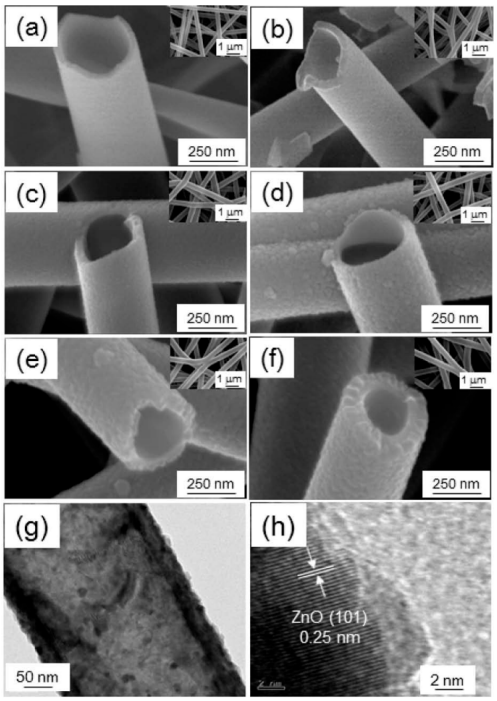

Figure 3. (**a**–**f**) Scanning electron microscope (SEM) images of TiO_2 hollow fibers synthesized with 1000 ALD cycles (**a**); TiO_2/ZnO double-layer hollow fibers synthesized with 20 ALD cycles (**b**); 50 ALD cycles (**c**); 90 ALD cycles (**d**); 220 ALD cycles (**e**); and 350 ALD cycles (**f**); (**g**) Transmission electron microscope (TEM) image of a single TiO_2/ZnO DLHF; (**h**) High resolution transmission electron microscopy (HRTEM) image of the outer layer ZnO [72]. Copyright 2014 American Chemical Society.

2.2. Solid Phase Reactions

Solid phase reactions are a quite facile process to synthesize composite sensing materials. In a typical process, pure powders are mixed uniformly using a physical method to electrostatically

self-assemble nanoheterostructures, which generally is a one-step procedure. For example, Zhou et al. have prepared Ag_2O/TiO_2 nanoheterostructures [73] through a solid phase reaction, where a certain amount of the pure Ag_2O and the corresponding amount of TiO_2 were uniformly mixed to get Ag_2O/TiO_2 nanoheterostructures. What's more, some other nanoheterostructures, such as polyaniline-titanium (PANi-TiO_2) nanoheterostructures [74], reduced graphene oxide/titanium dioxide (rGO/TiO_2) layered nanofilm [75], ZnO–TiO_2 nanocomposites [59], and TiO_2/SnO_2 nanocomposites [76], have also been successfully synthesized using this facile method.

2.3. Electrochemical Deposition

Compared with the CVD route, electrochemical deposition can obtain large-scale nanostructures at relatively low temperature. The conventional technique is very propitious to the fabrication of ordered, uniform, and highly dense nanoheterostructures for widespread applications. Recent years, some types of TiO_2-based nanoheterostructures are prepared using a two-step electrochemical deposition process [60,77]. In the deposition process, the pre-grown nanomaterials on fluorine-doped tin oxide (FTO), indium-doped tin oxide (ITO), or other relevant substrates are treated as working electrode for the following deposition. For instance, Yang and co-workers [78] have reported the preparation of the Cu-Cu_2O/TiO_2 nanocomposites via the electrochemical deposition method. The fabrication process consisted of two main steps: in the first step, helical TiO_2 nanotube arrays (NTAs) were prepared through anodizing a Ti foil. The second step was the electrodeposition of Cu and Cu_2O nanoparticles on the TiO_2 NTAs surface.

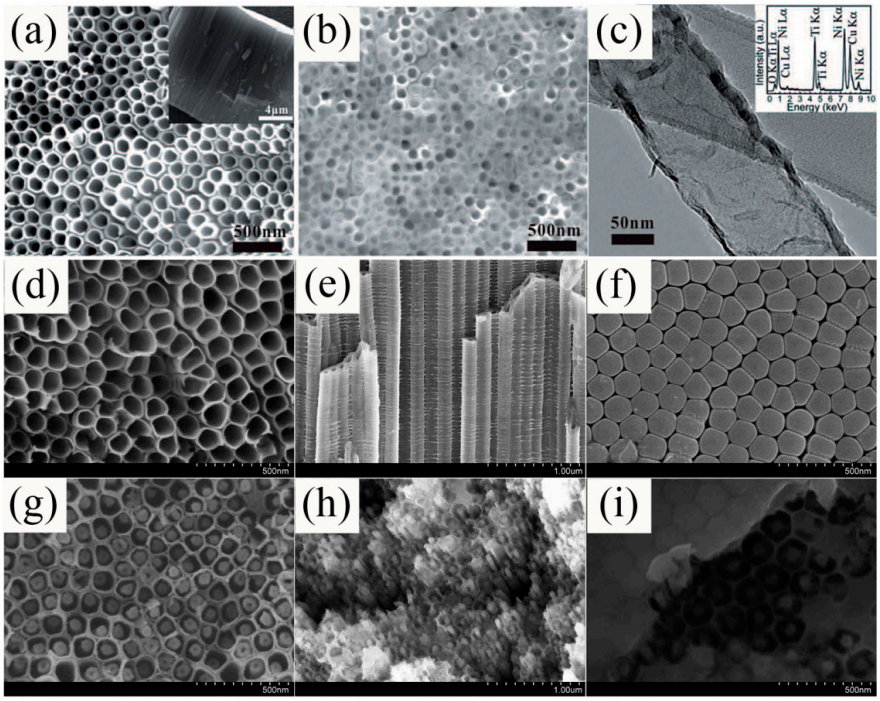

Figure 4. (**a**–**c**) SEM images of (**a**) TiO_2 NTAs and (**b**) hydrothermally treated TiO_2 NTAs; (**c**) TEM image of a typical $NiTiO_3/TiO_2$ NTs, the inset is the corresponding energy dispersive spectrometer (EDS) spectrum [79]. Copyright 2015 Wiley. (**d**–**i**) SEM images of as-anodized TiO_2 NTs (**d**–**f**) and TiO_2 NTs filled by Co-precursor nanorods (**g**–**i**) in top view(**d**,**g**), cross-sectional view (**e**,**h**), and bottom view (**f**,**i**) [80]. Copyright 2013 Royal Society of Chemistry.

Additionally, a great number of TiO_2-based nanoheterostructures were prepared using electrochemical deposition combined with other synthesis processes, where 1D TiO_2 arrays were commonly synthesized by electrochemical deposition, and then the as-prepared TiO_2 arrays would

be used as templates for heterostructure fabrication in the second synthesis step by other methods, including chemical deposition, hydrothermal/solvothermal methods, sol-gel method, and so on. For example, coaxial Ni/$NiTiO_3$/TiO_2 NTAs (Figure 4a–c) were synthesized by hydrothermally treating the as-anodized TiO_2 NTAs [79]. Nano-coaxial p-Co_3O_4/n-TiO_2 heterojunctions were synthesized first using electrochemical deposition and secondly using hydrothermal reaction [80]. The SEM images are shown in Figure 4d–i, where obviously the NTs with open top and closed bottom display high order and directionality. When soaking the as-anodized TiO_2 NTs in Co-based solutions, new nanorods with smaller diameter can be formed in the center of the TiO_2 NTs, representing the formation of nano-coaxial shaped of nanoheterostructures. Similarly, CdS/TiO_2 nanoheterostructures were fabricated by electrochemical deposition and sequential chemical deposition [81]; Pd/TiO_2 nanoheterostructures were synthesized by electrochemical deposition and a UV irradiation chemical method [82]; polypyrrole (PPy)/TiO_2 heterojunctions were fabricated by chemical deposition and electronchemical deposition methods [78,83].

2.4. Chemical Deposition

Chemical deposition is a convenient and low-cost technique for fabricating nanoheterostructures. For this method, the nanomaterials are obtained from the solid precipitation in the solution, and the concentration of the precursor, pH value, deposition temperature, and deposition time play important roles in the process. Nowadays, chemical deposition is generally applied in preparing either pure nanomaterials or composite nanomaterials. For example, brookite-TiO_2/a-Fe_2O_3 nanoheterostructures have been synthesized via two-step facile chemical deposition without using any templates or surfactants [65], as shown in Figure 5.

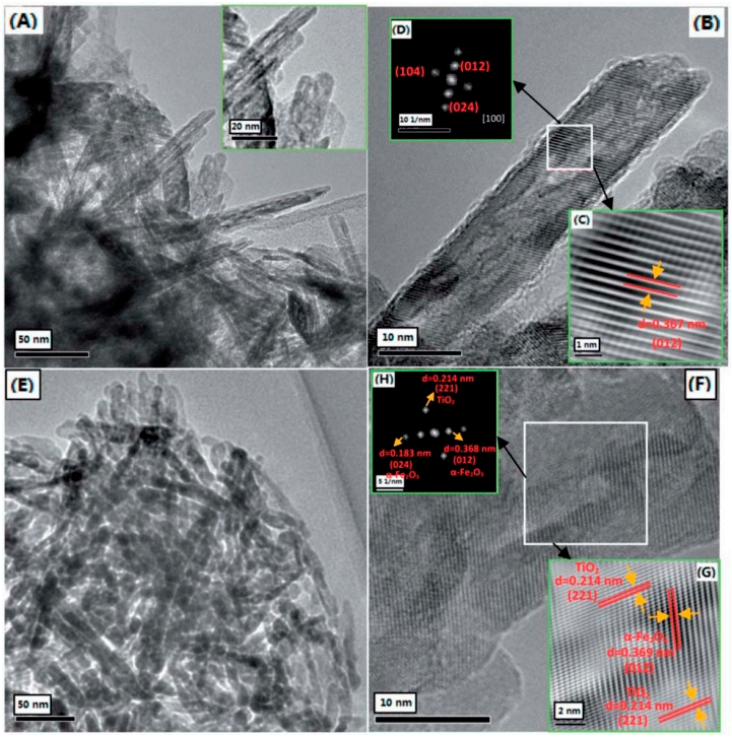

Figure 5. (**A**) TEM images of a-Fe_2O_3 nanorods; (**B**) HRTEM image of an individual a-Fe_2O_3 nanorod, the insets are the enlarged HRTEM image (**C**) and the corresponding fast Fourier transform (FFT) pattern (**D**) taken from the frame-marked region in (**B**); (**E**) TEM image of TiO_2/a-Fe_2O_3 nanoheterostructures; (**F**) HRTEM image of TiO_2/a-Fe_2O_3 nanoheterostructures, the insets are the enlarged HRTEM image (**G**) and the corresponding FFT pattern (**H**) taken from the frame-marked region in (**F**) [65]. Copyright 2014 Royal Society of Chemistry.

Furthermore, chemical deposition combined with other methods can also be used to fabricate nanoheterostructures. Our group has recently reported the fabrication of $Ag_2O/TiO_2/V_2O_5$ nanoheterostructures (STV NHs) [84] through a two-step synthesis approach: the first step was the preparation of continuous TiO_2/V_2O_5 nanofibers (TV NFs) using an electrospinning method, and the second step was the deposition of Ag_2O nanoparticles on the TV NFs surfaces by the reaction of $AgNO_3$ solution and NaOH solution. Based on this facile method, some other nanoheterostructures could be easily obtained, such as TiO_2/CuO [85], TiO_2/LiCl [86], and TiO_2/FeOOH [87] nanoheterostructures.

It is worthy to note that room temperature chemical method is an efficient way to synthesize organic-functionalized TiO_2 nanoheterostructures, such as TiO_2/polypyrrole nanocomposites [88], TiO_2-diltiazem/tetrachlorobismuth core-shell nanospheres (TiO_2@DTMBi core-shell nanospheres) [89], polymer-functionalized TiO_2 nanorods [90], molecularly imprinted polymer on TiO_2 nanotubes (MIP@TiO_2 NTs) [91], polypyrrole/TiO_2 heterojunction (PPy/TiO_2 heterojunction) [78], and Prussian blue/TiO_2 nanowires (PB/TiO_2 NWs) [63]. Typically, Wang and his co-workers [92] have reported a simple, low cost, and effective chemical method to fabricate polythiophene/Pd/TiO_2 ternary composite nanoheterostructures, where TiO_2 spheres were synthesized in water/acetone solvent, and then the Pd species were loaded on the TiO_2 microspheres, finally the polythiophene was covered on the spheres to obtain polythiophene/Pd/TiO_2 ternary composites.

2.5. Hydrothermal/Solvothermal Technique

Hydrothermal/solvothermal methods are commonly applied in the synthesis of powdery nanostructures. In the typical process, reagents (such as amines) and precursors are firstly mixed with each other in an appropriate ratio and then injected into a solvent, which can not only speed up the precursor dissolution but also accelerate the reaction between reagent and precursor. Finally the solution is added into a special hydrothermal synthesis reactor for the reaction of reagent and precursor and the growth of nanomaterials at relatively high temperature and high pressure. For example, TiO_2/V_2O_5 nanoheterostructures could be prepared through solvothermally treating TiO_2 nanoparticles in vanadium chloromethoxide precursor solution to growing V_2O_5 on TiO_2 nanoparticle surfaces [93]. Similarly, branched 1D α-Fe_2O_3/TiO_2 nanoheterostructures [62] were synthesized by growing α-Fe_2O_3 nanorods on the TiO_2 nanofibers using hydrothermal treatment. Figure 6 displays the SEM images of the branched α-Fe_2O_3/TiO_2 nanoheterostructures, it can be observed that the sample is mainly formed by branch-like nanofibers with loose and rough surfaces. In addition, one-dimensional carbon nanotube (CNT)-TiO_2 heterostructures were prepared through a solvothermal route using multiwalled CNTs as templates [25]. As demonstrated by these examples, hydrothermal/solvothermal methods are suitable techniques to fabricate controlled nanoheterostructures.

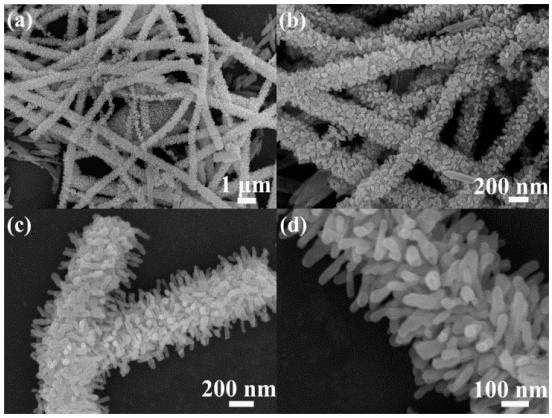

Figure 6. SEM images of branched α-Fe_2O_3/TiO_2 nanoheterostructures: (**a**,**b**) panoramic and (**c**,**d**) magnified [62]. Copyright 2013 American Chemical Society.

2.6. Sol-Gel Method

The sol-gel method is a representative wet chemistry technique for synthesizing TiO_2-based nanoheterostructures which involves relatively low growth temperatures and the morphology of the products can thus be controlled. The general process is as follows: first, prepare the sol gel, then heat the solution at high temperature combined with vigorous stirring to make it hydrolyze, finally carry out a condensation reaction to obtain nanomaterials. For instance, Lee et al. have fabricated a quartz crystal microbalance (QCZ) gas sensor based on the polyacrilic acid (PAA)/TiO_2 nanofilm, where the $(TiO_2/PAA)_n$ (n = 5, 10, and 20) nanofilms were deposited on gold-coated quartz crystal microbalance electrode using gas-phase surface sol-gel method [94].

2.7. Electrospinning

Since the electrospinning technique was first reported, more and more nanomaterials have been prepared by researchers via this simple method. During the typical process, a glutinous precursor solution is injected through a thin spinneret and then is stretched to form ultralong nanofibers; finally annealing the as-prepared samples at appropriate temperature can produce very highly crystalline nanofibers. In recent years, our group has successfully synthesized $TiO_2/Ag_{0.35}V_2O_5$ branched nanoheterostructures using a simple one-step electrospinning method [95,96]. The synthesis process of $TiO_2/Ag_{0.35}V_2O_5$ nanoheterostructures and characterization of the nanoheterostructures are presented in Figure 7.

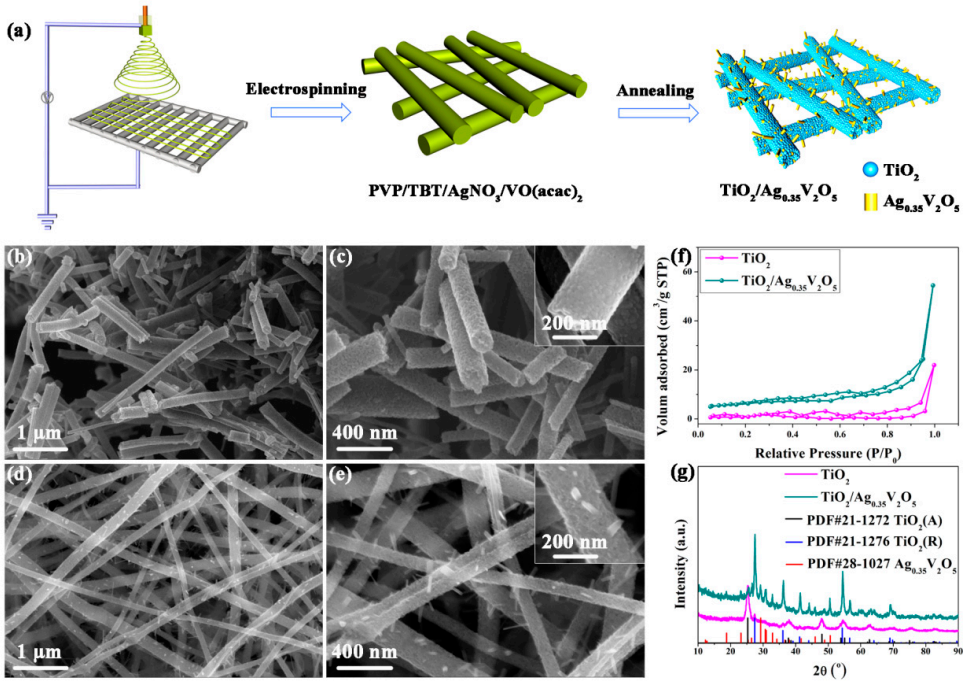

Figure 7. (**a**) A diagram of the electrospinning process; (**b**–**e**) SEM images of (**b**,**c**) TiO_2 nanofibers and (**d**,**e**) $TiO_2/Ag_{0.35}V_2O_5$ branched nanoheterostructures; (**f**) N_2 adsorption/desorption isotherms and (**g**) XRD patterns of TiO_2 nanofibers and $TiO_2/Ag_{0.35}V_2O_5$ branched nanoheterostructures [95]. Copyright 2016 Nature.

In the typical electrospinning process, the consistence of the composite, working voltage, inner diameter of the spinneret, distance between the spinneret tip and the collector substrate, and annealing temperature can all affect the morphology of the nanomaterials. Furthermore, Ag/TiO_2 and TiO_2/V_2O_5 nanoheterostructures have also been prepared using the electrospinning process by our group [97–99]. What's more, various type of TiO_2-based nanoheterostructures fabricated by electrospinning process

have been reported by other researchers, such as TiO_2/In_2O_3 [61], $LiCl/TiO_2$ [100], and Pt/TiO_2 [101] nanoheterostructures. Especially, Du's group has synthesized TiO_2/ZnO core-sheath nanofibers using a coaxial electrospinning method [102].

3. Diverse Nanoheterostructural Gas Sensors

During the past decades, TiO_2 has attracted considerable attention because it was regarded as a promising candidate for waste gas detection. Unfortunately, the poor sensing activity of high resistance n-type TiO_2 seriously influences the development of TiO_2-based gas sensors. Recently, various heterostructured sensing materials have been reported. The coupling of different materials can result in improved sensing activity. In this section, we will focus on the sensing performance of multifarious TiO_2-based nanoheterostructure gas sensors, highlighting in particular, semiconductor/semiconductor nanoheterostructures.

3.1. Semiconductor/Semiconductor Nanoheterostructures

One of efficient ways to devise outstanding gas sensors is the modification of TiO_2 by coupling with other semiconductors to form nanoheterostructures, which could display enhanced sensitivity and selectivity, faster response/recovery times, and/or lower operational temperatures than pure TiO_2 [45,46,100,103,104]. Table 1 summarizes the different TiO_2-based semiconductor/semiconductor nanoheterostructures and their performance in the gas sensing detection field. For example, Zeng et al. [105] have successfully fabricated a novel gas sensor based on the SnO_2-TiO_2 hybrid nanomaterials.

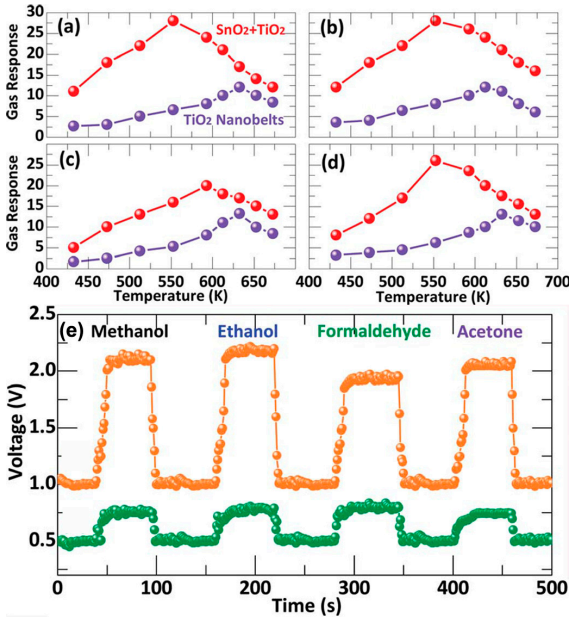

Figure 8. (**a**–**d**) Gas response of the TiO_2 nanobelts and the SnO_2-TiO_2 hybrid oxides based sensors to 400 ppm methanol (**a**); ethanol (**b**); formaldehyde (**c**); and acetone (**d**) gases at different operating temperatures; (**e**) Response/recovery characteristics of the TiO_2 nanobelts and the SnO_2-TiO_2 hybrid oxides based sensors operated at 593 K to 400 ppm methanol, ethanol, formaldehyde, and acetone [105]. Copyright 2012 Royal Society of Chemistry.

They demonstrated that the SnO_2 nanospheres-functionalized TiO_2 nanobelts-based sensor displayed very outstanding sensing properties, higher response and lower operating temperature, than pure TiO_2 nanobelts-based sensors, as shown in Figure 8.

Table 1. Summary of the gas sensing properties of TiO_2-based semiconductor/semiconductor nanoheterostructure sensors.

TiO_2-Based Nanoheterostructures	Fabrication Method	Size	Detection Gas	Detection Range	Response				Ref.
					Operation Temperature (°C)	Sensitivity	Response/ Recovery Time	Concentration	
TiO_2/Co_3O_4 acicular nanowires	hydrothermal + pulsed laser deposition	length: 1–3 μm; diameter: 200 nm	ethanol	10–500 ppm	160	R_g/R_a: 65		100 ppm	[106]
nano-coaxial p-Co_3O_4/n-TiO_2 heterojunction	electronchemical anodization + hydrothermal process	nanotubes diameter: ~150 nm; core nanorods diameter: ~50 nm	ethanol		260	R_a/R_g: 40	1.4/7.2 s	100 ppm	[80]
Fe_2O_3/TiO_2 tube-like nanostructures	hydrothermal + chemical deposition	diameter: 120 nm; length: 400 nm; outer wall thickness: 23.5 nm	ethanol	0.5–500 ppm	270	R_a/R_g: 19.4		500 ppm	[107]
SnO_2-coated TiO_2 nanobelts	hydrothermal	TiO_2 nanobelts: length: over ten micrometers; width: 100–200 nm; thickness: 20–40 nm; SnO_2 nanoplates: length: 20–200 nm; thickness: 20 nm	ethanol	10–500 ppm	43	R_a/R_g: 11.2	40/5 min	10 ppm	[108]
TiO_2/SnO_2 core shell nanocomposites	hydrothermal treatment + chemical deposition		ethanol	500–5000 ppm	200	R_a/R_g: 12.7	≤50/50 s	1000 ppm	[109]
SnO_2 nanospheres functionalized TiO_2 nanobelts	hydrothermal process	nanobelts diameter: 50–200 nm; length: several micrometers; nanospheres diameter: ~400 nm	ethanol	100–800 ppm	320	R_g/R_a: 27.5		400 ppm	[105]
Ag-TiO_2/SnO_2 nanocomposites	chemical deposition	diameter: ~100 nm	ethanol	1–500 ppm	275	R_a/R_g: 53	3.5/7 s	50 ppm	[104]
TiO_2/V_2O_5 nanoheterostructures	electrospinning	nanobranches diameter: 15–20 nm; nanofibers diameter: 160 nm	ethanol	20–1000 ppm	350	R_a/R_g: 24.6	6/7 s	100 ppm	[97]
$TiO_2/Ag_{0.35}V_2O_5$ branched nanoheterostructures	electrospinning	nanobranches diameter: ~20 nm; nanofibers diameter: ~190 nm	ethanol	20–1000 ppm	350	R_a/R_g: 31.8	7/12 s	100 ppm	[95]
brush-like ZnO-TiO_2 heterojunctions nanofibers	electrospinning + hydrothermal process	ZnO nanorods diameter: 100–300 nm; TiO_2 nanofibers diameter: 100 nm	ethanol	20–500 ppm	320	R_a/R_g: 50.6	5/10 s	500 ppm	[110]
TiO_2/ZnO core-shell nanorods	hydrothermal method + ALD	core width: 120 nm; shell width: 20 nm	ethanol	5–25 ppm	150	R_a/R_g: 2.37	100/70 s	10 ppm	[64]
ZnO surface functionalized TiO_2	electrospinning + hydrothermal treatment	nanofibers diameter : 70–100 nm; ZnO nanosheets diameter: 500 nm	ethanol	10–200 ppm	280	R_a/R_g: 15.7	5/3 s	100 ppm	[111]
ZnO/TiO_2 nanocomposites	CVD		ethanol		400	R_a/R_g: 5	~1/1 min	50 ppm	[46]
brookite TiO_2 decorated a-Fe_2O_3 nanoheterostructures	chemical deposition	length: 50–100 nm; diameter: ~10 nm	butanol	10–500 ppm	370	R_a/R_g: 27.6	5/6 s	100 ppm	[65]
ZnO-TiO_2 nanocomposites	CVD	diameter: 5–20 nm	acetone	20–100 ppm	350	R_a/R_g: 22.7	1/1 min	100 ppm	[46]
ZnO/TiO_2 nanocomposites	CVD		acetone			R_a/R_g: 22		100 ppm	[46]
CuO-TiO_2 heterostructure nanofibers	electrospinning + hydrothermal process	TiO_2 nanofibers: length: several tens micrometers; diameter: 200 nm; CuO nanocubes: diameter: 40–80 nm	formaldehyde	5–100 ppm	200	R_a/R_g: 15.5		50 ppm	[112]
Cd/SnO_2/TiO_2 composites	sol-gel		formaldehyde	100–500 ppm	320	R_a/R_g: 32	25/17 s	200 ppm	[113]
α-Fe_2O_3/TiO_2 branch-like hierarchical heterostructures	electrospinning + hydrothermal method	diameter: 600 nm; length: several micrometers	trimethylamine	10–200 ppm	250	R_a/R_g: 13.9	0.5/1.5 s	50 ppm	[62]
hierarchically assembled ZnO nanorods on TiO_2 nanobelts	hydrothermal process	TiO_2 nanobelts: width: 50–200 nm; length: several micrometers; ZnO nanorods: length: 500 nm	trimethylamine	5–500 ppm	200	R_a/R_g: 25		5 ppm	[114]
SnO_2/TiO_2 composites	sol-gel		methanol	50–400 ppm	360	R_a/R_g: 60	10–15/14–20 s	200 ppm	[115]

Table 1. *Cont.*

TiO_2-Based Nanoheterostructures	Fabrication Method	Size	Detection Gas	Detection Range	Response				Ref.
					Operation Temperature (°C)	Sensitivity	Response/ Recovery Time	Concentration	
ZnO-TiO_2 nanocomposites	physical mixture		humidity	5%–90% RH	RT (room temperature)	(ΔR)/(Δ%RH): 9.08 MΩ/%RH			[59]
LiCl/TiO_2 electrospun nanofibers	electrospinning	diameter: 150–260 nm	humidity	11%–95% RH	RT	R_a/R_g: 10^3	<3/7 s	11%–95% RH	[100]
$ZnSnO_3$ nanoneedles/TiO_2 nanofibers heterojunction	electrospinning + hydrothermal treatment	TiO_2 nanofibers diameters: 200–300 nm; $ZnSnO_3$ nanorods: tip diameter: 0.5~1.5 nm; ratio of length to diameter: ~9.6	humidity	11%–95%	RT		2.5/3 s		[116]
$ZnSnO_3$ nanoparticles/TiO_2 nanofibers heterojunction	electrospinning + hydrothermal treatment	TiO_2 nanofibers diameters: 200–300 nm; $ZnSnO_3$ nanoparticles diameters: 30–50 nm	humidity	11%–95%	RT		3.5/29 s		[116]
Ce_2O_3/TiO_2/SnO_2 thin film	sol-gel		humidity	15%–95% RH	RT	R_a/R_g: 100		40%	[117]
polypyrrole-coated TiO_2/ZnO nanofibers	electrospinning + chemical deposition	TiO_2/ZnO core diameter: 100 nm; PPy shell thickness: 7 nm	NH_3	0.5–450	RT	$\Delta R/R_a$: 0.35		450 ppm	[118]
nanocrystalline TiO_2/SnO_2 composites	commercial powder		NH_3	100–5000 ppm	400	$\Delta R/R_a$: 0.5		1200 ppm	[119]
SnO_2/TiO_2nanoneedles	wet chemical method	diameter: 40–80 nm; length: 60–100 nm	NH_3		150	$(\Delta R/R_g) \times 100\%$: 300%	3/5 min	1000 ppm	[120]
TiO_2/SnO_2 thick film	sol		NH_3	100–1000 ppm	250	R_a/R_g: 3		400 ppm	[121]
TiO_2/ZnO inner/outer double-layer hollow fibers	electrospinning + ALD	inner diameter: ~320 nm; TiO_2 layer thickness: ~30 nm; ZnO outer layer thickness: 20 nm	CO	0.1–10 ppm	375	R_a/R_g: 20.3		1 ppm	[72]
TiO_2/Fe_2O_3 nanosized thin film	sputtering	diameter: 20–30 nm	CO			$\Delta R/R_a$: 15	~50/- s	1000 ppm	[122]
TiO_2/Al_2O_3/Pd composites	sol		H_2S	200–1000 ppm	225	$\log(R_a/R_g)$: 0.9		1000 ppm	[48]
nanocrystalline CdO/ZnO/TiO_2	pyrolyzation		H_2S		225–250	$\Delta R/R_a$: 0.8		10,000 ppm	[123]
TiO_2 decorated CuO nanorods	thermal evaporative + sputtering	diameters: 50–100 nm; lengths: a few tens of micrometers	H_2	0.1–5 ppm	300	R_a/R_g: 8.57		5 ppm	[124]
TiO_2/SnO_2 nanocomposites	physical mixture	diameter: 8–28 nm	H_2	50–3000 ppm	375				[76]
TiO_2 fibers supported β-FeOOH nanostructures	electrospinning + hydrothermal method	nanofiber diameter: ~500 nm	H_2	100 500 ppm	RT	R_a/R_g: 52.5		500 ppm	[87]
mesoporous Nb_2O_5/TiO_2	sol-gel	diameter: 4.1 nm	H_2		450	R_a/R_g: ~5.5	~1/1 min	500 ppm	[125]
TiO_2/NiO thin film	sputtering		H_2	200 ppm–0.5%	300	R_g/R_a: 15	2/2.3 min	1000 ppm	[126]
PtO/Pt/TiO_2 thin film	sol-gel		H_2	1%–10%	180	$\Delta R/R_a \times 100\%$: 40%	~10/10 min	2%	[103]
TiO_2-In_2O_3 composite nanofibers	electrospinning	diameters: 250 nm; length: several micrometers	NO_2	0.3–97 ppm	RT	$\Delta R/R_a$: ~1.25	~9.5/- s	1 ppm	[61]
SnO_2-core/V_2O_5-shell nanorods	thermal evaporation + sputtering	length: several tens micrometers; SnO_2-core thicknesses: 100 nm; V_2O_5-shell thickness: 10 nm	NO_2	10–80 ppm	300	R_g/R_a: 1.03%	≤4.5/4.5 min	10 ppm	[127]
Al_2O_3 decorated anatase TiO_2 nanotubes	electrochemical anodization + thermal decomposition	nanotube outer diameter: ≤200 nm; length: several micrometers	NO_x	0.97–97 ppm	RT	$\Delta R/R_a$: 88.04%	8/- s	97 ppm	[45]
CuO-TiO_2-Au nanosystems	CVD + sputtering		O_3					300 ppb	[71]
V_2O_5/TiO_2 thin film	sol-gel	3–5 nm	O_2	1 ppm–20.9%	250	R_g/R_a: 3.5	5/30 min	120 ppm	[128]
CeO_2/TiO_2 thin film	sol-gel		O_2	5–10,000 ppm	420	R_g/R_a: ~3	40–60/80	1000 ppm	[129]
SnO_2/TiO_2 thin film	sputtering	44–67 nm	O_2	100–2000 ppm		R_g/R_a: 2		1000 ppm	[130]

Tomer and Duhan [104] reported a mesoporous Ag-(TiO_2/SnO_2) structure which exhibited high sensitivity, a low detection limit (1 ppm), and wide detection range (1 ppm to 500 ppm) to ethanol, as shown in Figure 9. Moreover, the mesoporous Ag-(TiO_2/SnO_2) nanohybrid sensor also displayed excellent stability and high selectivity for ethanol.

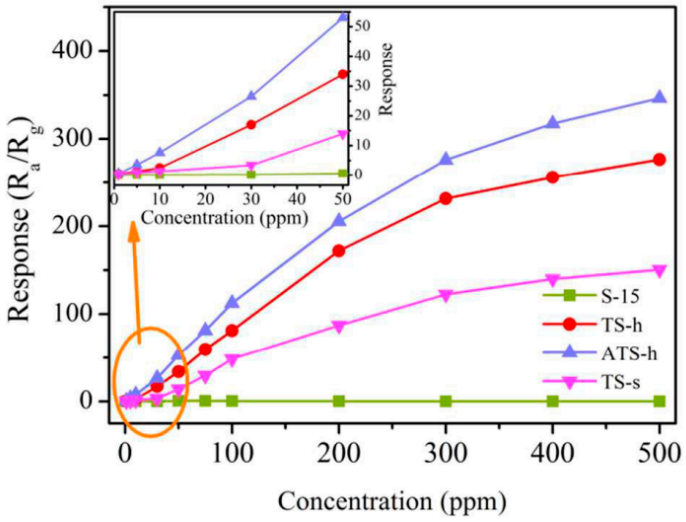

Figure 9. Gas responses of different sensors (S-15: SBA-15, TS-s: TiO_2/SnO_2 (soft template), TS-h: TiO_2/SnO_2 (hard template), ATS-h: Ag-(TiO_2/SnO_2)) to ethanol operated at 275 °C, the inset is the calibration curve within the concentration ranging from 1 ppm to 50 ppm [104]. Copyright 2016 Royal Society of Chemistry.

3.1.1. Sensing Mechanism

Although the mechanism of the heterostructures has not been investigated explicitly, it is clear that the enhanced sensing properties for semiconductor/semiconductor nanoheterostructures should be related to the heterojunction constracted at the interface between two semiconductors, where the changes of heterojunction energy barrier immerged into different gas atmospheres are benefit to the improvement of sensing properties.

One possible explanation for the enhancement of these heterostructure-based sensors is the heterojunctions formed between TiO_2 and other semiconductors. On the basis of band atructures and conductivity type of the semiconductors, two main types of semiconductor/semiconductor heteroatreuctures, n-n heterojunctions and p-n heterojunctions, can be considered. The work function (highest potential of valence band (VB)), electron affinity (lowest potential of CB), and bandgap of the coupled semiconductors determine the electron/hole dynamics in the heterojunctions. Since the work function of TiO_2 is different from that of coupling semiconductors, the electrons will transfer from one semiconductor to another, thus resulting in an additional depletion layer and an energy barrier at the interfaces of two semiconductors. Compared with the pure semiconductors, the conductivity of heterojunctions is mainly detrermined by the energy barrier, and the relationship between resistance and energy barrier of the heterojunctions can be presented by the following equation:

$$R \propto B\, exp(q\Phi/kT) \tag{3}$$

where B is a constant, k is the Boltzmann constant, T is the absolute temperature, and $q\Phi$ is the effective energy barrier at the heterojunction. When the heterostructures are in an air atmosphere, the electrons can be adsorbed by oxygen molecules to turn into various oxygen ions including O^-, O^{2-}, and $O_2{}^-$, accordingly the height of the energy barrier in heterojunctions will increase, as shown in the first figure of Figure 10a. Similarly, the energy barrier height will further increase when put into oxidizing

gases, whereas in reducing gases, the gases can react with the oxygen ions and result in the release of adsorbed electrons, therefore the energy barrier height will decrease, as shown in the second figure of Figure 10a. According to Equation (3), R_a/R_g is proportional to $\exp(\Delta q\Phi)$, thus the notable changes of energy barrier height can cause remarkable changes of the resistivity and superior enhancement of sensing properties for heterojunctions. For instance, Fe_2O_3/TiO_2 tube-like nanoheterostructures [107] and $TiO_2/Ag_{0.35}V_2O_5$ branched nanoheterostructures [95] based sensors exhibited improved ethanol sensing performance compared with pure matrix sensors.

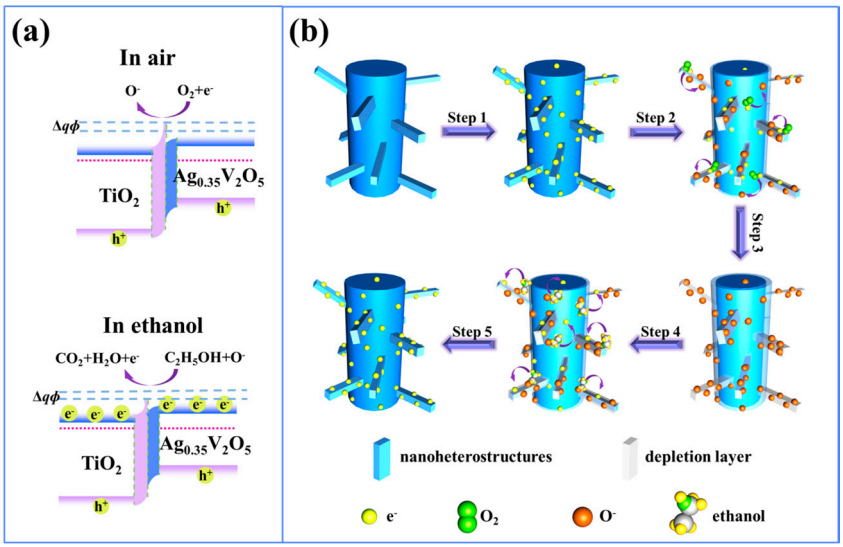

Figure 10. The proposed sensing mechanism diagram of $TiO_2/Ag_{0.35}V_2O_5$ nanoheterostructures. (**a**) Schematic band structure of $TiO_2/Ag_{0.35}V_2O_5$ heterojunction exposed in air and ethanol gases ($q\Phi$: energy barrier); (**b**) Sensing model of the $TiO_2/Ag_{0.35}V_2O_5$ nanoheterostructured sensor in air (Steps 1–3) and in ethanol (Steps 4–5) [95]. Copyright 2016 Nature.

Additionally, a synergetic effect between different nanomaterials is also regarded as one of important reasons for the enhanced sensing properties of nanoheterostructures. In fact, the synergetic effect is related only to the situation where both of the pure materials exhibit high sensitivity to the tested gases [61].

It is well known that some metal oxide semiconductors are effective catalysts which can help decompose organic gases. Therefore, the catalytic effect of TiO_2 and other materials should be taken into account in the sensing performance enhancement of nanoheterostructures. For example, according to the previous reports by our group [98,131], the TiO_2/V_2O_5 nanoheterostructures can act as much more effective catalysts than pure TiO_2 nanofibers, and should be capable of promoting the sensing reaction between volatile organic solvents (VOCs) and oxygen ions adsorbed at the surface, thus a TiO_2/V_2O_5 nanoheterostructures-based ethanol sensor displays much higher sensitivity than a pure TiO_2-based sensor [97].

In addition to the heterojunction effect, synergetic effect, and catalytic effect, there may be other mechanisms in play for enhancing the sensing performance of nanoheterostructure. For example, Chen et al. [108] considered that the electron transfer are facilitated because of the formation of SnO_2/TiO_2 heterostructures, thus the gas sensing response including sensitivity and selectivity is efficiently enhanced as a result of increased charge carrier concentration.

Actually, there is more than one reason for the enhanced mechanisms of nanoheterostructure sensors. Park and coworkers [64] demonstrated that the improved ethanol sensing performance of TiO_2-core/ZnO-shell nanorods compared with that of pure TiO_2 nanorods might be due to more efficient catalytic activity of ZnO and the potential barriers built in the heterojunctions. Wang and coworkers [61] found that the improved gas sensing activity of the porous single crystal In_2O_3

beads@TiO_2-In_2O_3 composite nanofibers (TINFs) could be ascribed to the Schottky junction formed between single crystal In_2O_3 beads and the Au electrode, the increased carrier density derived from the TiO_2 electron-donor, and the best gas absorption conditions provided by the surface-related defects, as shown in Figure 11.

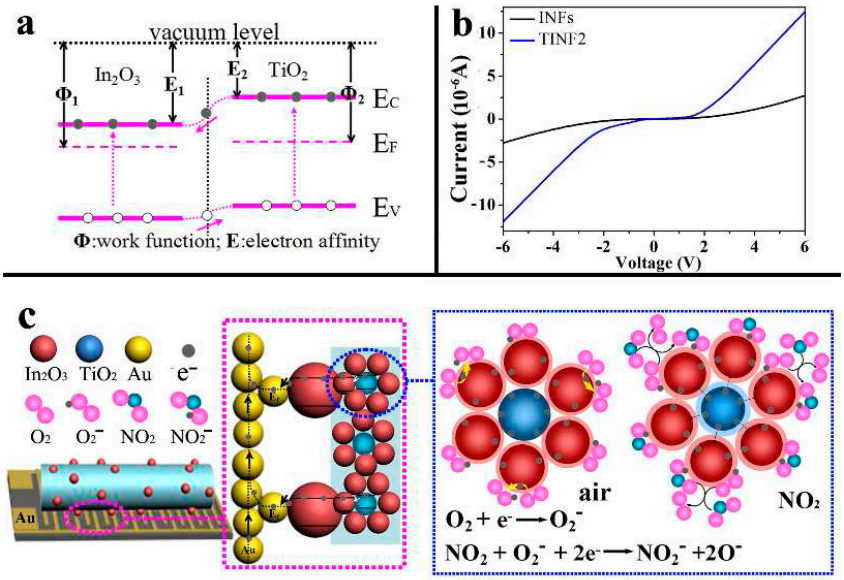

Figure 11. (**a**) Energy band diagram of In_2O_3 and TiO_2, E_C: conduction band, E_V: valence band; (**b**) I-V curves of In_2O_3 nanofibers (INFs) and In_2O_3 beads@TiO_2-In_2O_3 composite nanofibers (TINF2) thin film sensors in air at room temperature (the gate voltage Vg = 0.1); (**c**) The gas sensing reactions based on Schottky junction between Au electrode and In_2O_3 beads [61]. Copyright 2015 American Chemical Society.

3.1.2. The Influence of Morphology on Sensing Performance

It is reasonable that the influence of nanoheterostructures morphology on sensing performance should be taken into account, where the gas sensitivity and the response/recovery time affected by gas absorption and gas diffusion can be improved by the large specific surface area and the especial morphology of materials. On the one hand, like for resistance-type gas sensors, the fundamental sensing process is the reaction of the target gases and the electrons at the surface of the sensing materials. Larger surface area means more surface active sites can be provided for gas absorption and reactions, resulting in more noticeable changes of resistance in different gases, consequently the sensitivity of the sensors can be improved. On the other hand, the electron exchange process can only occur within a thin layer, the width of this surface layer is determined by the Debye length (L_D) of the materials, which is defined by following equation:

$$L_D = \left(kT\varepsilon\varepsilon_0/q^2 n_c\right)^{1/2} \quad (4)$$

where T is the absolute temperature in Kelvin, k is Boltzmann's constant, ε_0 is the permittivity of vacuum, ε is the static relative dielectric constant, n_c is the carrier concentration, and q is the electrical charge of the carrier. When L_D is less or equivalent to the thickness of the nanostructures, the electrons in semiconductors can be totally depleted by the oxygen molecules adsorbed on the surface, thus will result in more evident resistance change after exposure in gases compared with that of not entirely depleted ones.

Hierarchical nanostructures are a particularly promising choice for further enhancing the sensing performance because of their extremely large specific surface area and/or thin thickness (less or

equivalent to L_D). As a matter of fact, several hierarchical TiO_2-based nanoheterostructures, such as branch-like α-Fe_2O_3/TiO_2 hierarchical heterostructure [62], hierarchically assembled ZnO nanorods on TiO_2 nanobelts [114], SnO_2 nanospheres functionalized TiO_2 nanobelts [105], have been fabricated into gas sensors. In particular, Zhu and coworkers have reported that β-FeOOH/TiO_2 hierarchical heterostructures exhibited remarkably high sensitivity and reversibility [87]. Our group [95] demonstrated that the enhancement of the TiO_2/$Ag_{0.35}V_2O_5$ gas sensor could be attributed to the extraordinary branched-nanofiber structures with large surface area and thin branch diameter (the semidiameter of the branches was equivalent to the depletion layer of the $Ag_{0.35}V_2O_5$), where more gas molecules could be absorbed and electrons in the $Ag_{0.35}V_2O_5$ nanobranches could be totally depleted by the oxygen molecules adsorbed on the surface (Figure 10b). Furthermore, Deng et al. [110] have found that the enhanced performance of the ZnO-TiO_2-based gas sensors could be ascribed to the hierarchical structures, as shown in Figure 12, where the high specific surface area could result in a large number of gas molecules absorbed on the surface of ZnO-TiO_2 nanoheterostructures when compared with the pure TiO_2 nanofibers, additionally, well aligned structures of the nanoheterostructures would cause the unhindered gas diffusion to the whole surface of the sensor.

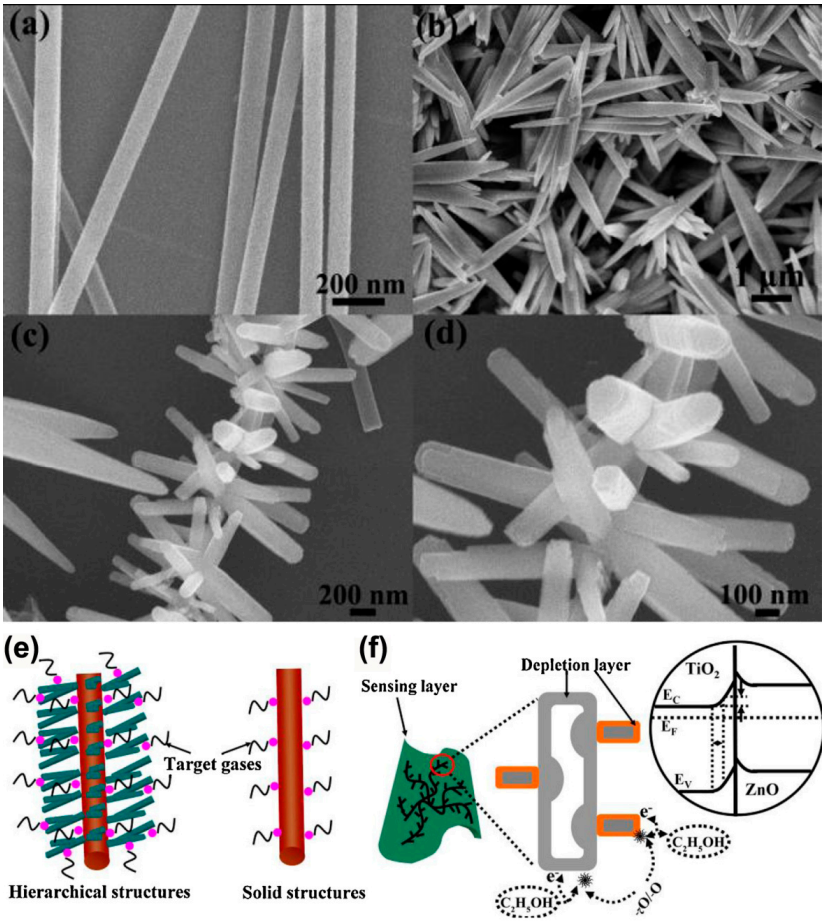

Figure 12. (**a**–**d**) SEM images of TiO_2 nanofibers (**a**); ZnO nanorods (**b**); and ZnO-TiO_2 nanoheterostructures (**c**,**d**); (**e**,**f**) Schematic diagram of catalytic reactions (**e**) and ideal band structure (**f**) of ZnO-TiO_2 nanoheterostructures [110]. Copyright 2013 Elsevier.

In addition to island type hierarchical heterostructured sensors, core/shell type and hollow type nanoheterostructures have also attracted much attention in gas sensor research. Recently, Zhu et al. [107] synthesized tube-like Fe_2O_3/TiO_2 core/shell nanoheterostructures (Figure 13). The special core/shell nanoheterostructures could act as a superior ethanol sensor material with

respect to the pristine one, as shown in Figure 13. Katoch and coworkers [72] demonstrated that TiO_2/ZnO double layer hollow fibers exhibited superior CO sensing performance compared to the ZnO single layer hollow fibers, as shown in Figure 14a. The enhancement was ascribed to the fact that the electrons in ZnO outer layer could be easily absorbed to TiO_2 inner layer, thus ZnO would become more resistive owing to the noticeable loss of electrons, as shown in Figure 14b,c. When exposed in CO gas atmosphere, the resistance of ZnO outer layer would partially regain its original value, this could lead to more noticeable resistance change for the TiO_2/ZnO double layer hollow fibers in detecting CO gas.

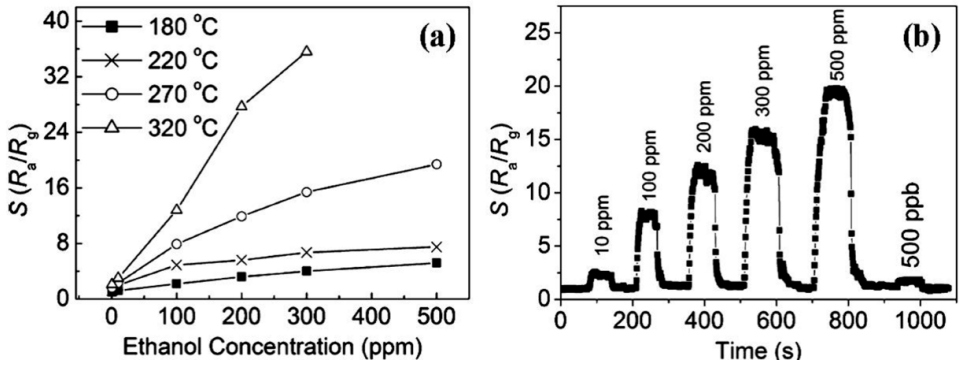

Figure 13. (**a**) Sensing response of the Fe_2O_3/TiO_2 tube like nanoheterostructures to ethanol at different temperatures; (**b**) Time dependent sensing response of the Fe_2O_3/TiO_2 tube like nanoheterostructures to ethanol vapor at 270 °C [107]. Copyright 2012 American Chemical Society.

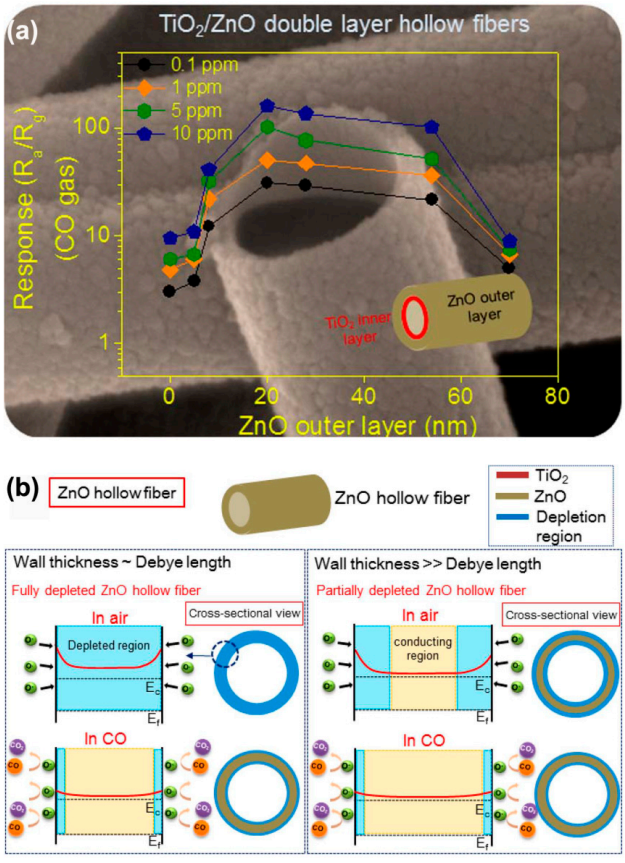

Figure 14. *Cont.*

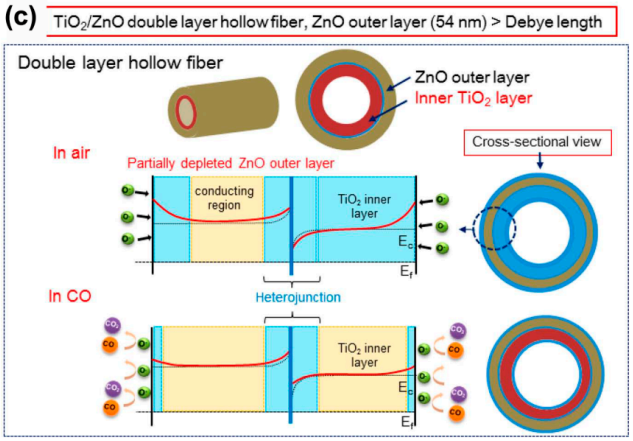

Figure 14. (**a**) Sensing response of TiO_2/ZnO double layer hollow fibers to CO gas as a function of ZnO outer layer thickness; (**b**,**c**) Schematic diagrams of sensing mechanism of (**b**) ZnO hollow fibers and (**c**) TiO_2/ZnO double-layer hollow fibers [72]. Copyright 2014 American Chemical Society.

3.2. Carbon-Group-Materials/Semiconductor Nanoheterostructures

The formation of carbon-group-materials/semiconductor heterostructures is also an important technique to improve the gas sensing performance of TiO_2. In recent years, carbon-group-materials have attracted much attention for applications in gas sensors [1,12,15,132]. The nanostructured carbon materials including carbon nanotubes (CNTs) and graphene possess outstanding physical, chemical and electrical properties, such as good flexibility, large surface area, high chemical stability, and high electrical conductivity [14,133]. These excellent features make them extremely suitable for use as candidates in enhancing semiconductors' sensing properties [132,134–136]. It has been demonstrated that the absorptivity, conductivity, and/or electrochemical reaction of some small gas molecules of carbon/TiO_2 nanoheterostructures could be promoted, thus the nano- heterostructures can display remarkably improved sensing performance [75,137–139]. Table 2 summarizes the carbon/TiO_2 nanoheterostructures and their performance in the detection of gases.

The mechanism of enhanced gas sensing performance of the carbon/TiO_2 nanoheterostructures is proposed to occur as follows: first, carbon-group-materials possess huge specific surface areas and nanoscale structures, thus a large number of surface sites are exposed for reacting with gases, therefore various gases can be easily detected at lower operating temperatures [140,141]. Second, the electric conductivity of carbon-group-materials is much higher in comparison with TiO_2, this can reduce the resistance and enhance the electrons transport capability of heterostructured sensors, thus making the nanoheterostructures based sensors work at lower operating temperature [142,143]. Third, since TiO_2 displays n-type semiconductor characteristic and carbon group- materials (graphene, CNTs) display p-type semiconductor characteristic, hence, a competitive mechanism may occur surrounding the carbon-group-materials/TiO_2 heterojunctions, which can lead to enhanced gas sensitivity owing to the decrease of the work function (barrier height) or increase of the conductivity of TiO_2 sensitive layer [144,145]. Furthermore, the catalytic activity of TiO_2 should also be considered as one of important reasons for the improved sensing performance of carbon-group-materials/TiO_2 nanoheterostructures [146,147].

As an emerging carbon material, graphene is regarded as a promising candidate for application in gas sensors due to its huge surface area, high electrical conductivity, inherently low electrical noise, environmental ultra-sensitivity, and ease microfabrication. In particular, the combination of graphene and TiO_2 can achieve efficiently improved sensing performance.

Table 2. Summary of the gas sensing properties of carbon-group-materials/TiO_2 nanoheterostructure sensors.

TiO_2-Based Nanoheterostructures	Fabrication Method	Size	Detection Gas	Detection Range	Response				Ref.
					Operation Temperature (°C)	Sensitivity	Response/ Recovery Time	Concentration	
Pd/TiO_2/reduced graphene oxide ternary composite	one-pot polyol		NH_3	5–150 ppm	RT	$(\Delta R/R_a) \times 100\%$: 39.9%		100 ppm	[142]
PPy/graphene nanoplatelets decorated TiO_2 nanoparticles	sol-gel + chemical polymerization	TiO_2 nanoparticles diameter: 10–30 nm	NH_3	1–200 ppm	RT	$(\Delta R/R_a) \times 100\%$: 102.2%	36/16 s	50 ppm	[146]
CNTs/TiO_2 nanocomposites	screen-printing + dip-coating techniques		NH_3		RT	$\Delta R/R_a$: 93	9/2 min	1%	[148]
Pt/TiO_2/MWCNTs nanocomposites	sol-gel		H_2	5%–100%	50	$(\Delta R/R_a) \times 100\%$: 30%		70%	[149]
CNTs/Pt-TiO_2 NTs	anodization	diameter: 100 nm;length: 14 um	H_2	0.5%–3%	100	$(\Delta R/R_a) \times 100\%$: 2%		1%	[150]
Pt-TiO_2/MWCNTs hybrid composites	wet chemical procedure		H_2	0.5%–3%	150			0.5%	[140]
rGO/TiO_2 thin film			formaldehyde	0.1–1 ppm	RT	$(\Delta R/R_a) \times 100\%$: 0.64	70/126 s	1 ppm	[75]
MWCNTs/TiO_2 nanocomposites	sol-gel	diameter: 20–40 nm	CO		350	R_a/R_g: 15.8	4/16 s	50 ppm	[151]
MWCNTs/TiO_2 thin film	sol-gel		CO		400	R_a/R_g: 89.2	5.16/2.72 s	100 ppm	[152]
graphene-TiO_2 nanocomposite	sol–gel	TiO_2 nanoparticles: ~35 nm	CO_2	500–15,000 ppm	200	R_g/R_a: 1.34		10,000 ppm	[144]
TiO_2/carbon black	sol-gel		NO_2	1–100 ppm	150	$\Delta R/R_a \times 100\%$: 7%		100 ppm	[153]
single-walled carbon nanotube/TiO_2 hybrid		length of carbon nanotubes: 20–50 nm	NO	50 ppb–1 ppm	RT	$(\Delta R/R_a) \times 100\%$: 9%		50 ppb	[140]
CNT/TiO_2 hybrid films	sol-gel		O_2	10 ppm	350	$\Delta R/R_a$: 6.5	8/- s	10 ppm in CO_2	[154]
grapheme oxide/nano-anatase TiO_2		~5 nm	humidity	35%–95%		power loss/ΔRH: ~0.47 dB/%RH	0.74/0.91 s		[141]

In Ye's research [75], rGO/TiO_2 layered thin film were prepared on the interdigital electrode substrates via a spray method. Formaldehyde sensing tests demonstrated that the layered thin film exhibited high sensitivity (0.905 ppm^{-1}), and a reversible and linear response to 0.1–0.5 ppm formaldehyde at room temperature, and that this could be ascribed to the positive synergetic effect of the two materials, as shown in Figure 15. Xiang and coworkers [146] developed a room-temperature sensitive NH_3 gas sensor using TiO_2@PPy-graphene nanocomposites. The sensor displayed high sensitivity (102.2%), superior reproducibility, and excellent selectivity to 50 ppm NH_3. Additionally, Wang et al. [147] synthesized TiO_2/graphene composite film for O_2 sensing upon exposure to UV light. They found that the outstanding sensitivity of the composite film could be ascribed to the synergetic effect of the ultrasensitivity of single-layer graphene to the environment and photocatalytic activity of TiO_2.

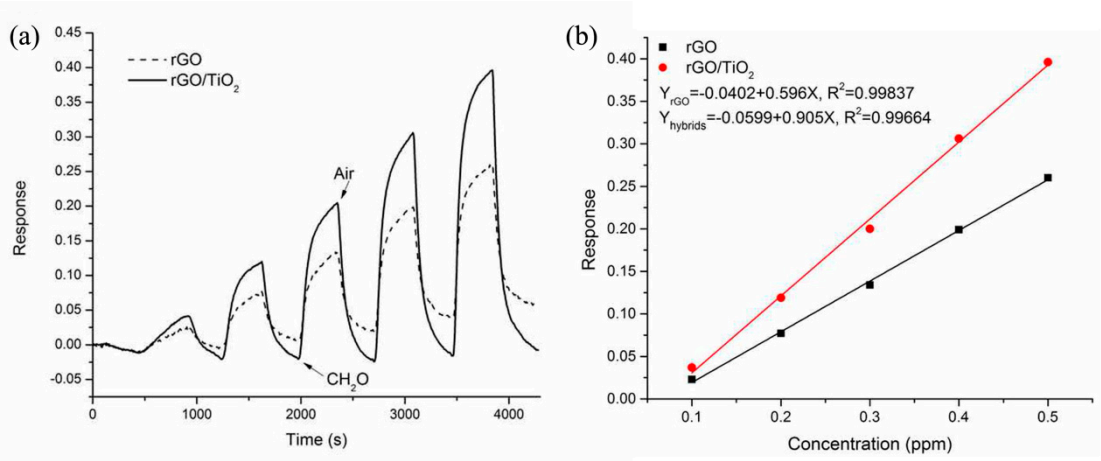

Figure 15. (**a**) response curves and (**b**) response values of pure rGO and rGO/TiO_2 layered films to 0.1–0.5 ppm CH_2O [75]. Copyright 2015 Elsevier.

Like graphene, CNTs have also been widely studied as preeminent gas sensing materials. Recently, multifarious effort has been devoted to the design and fabrication of CNTs/metal oxide nanocomposites [138,139,149,155]. The new composite materials will maintain the original properties of each component, or even show a synergistic effect, which is exceedingly significate to sensing performance. For example, Llobet et al. [154] proposed an effective O_2 sensor based on CNTs/TiO_2 hybrid films. The researchers compared the sensing properties of CNTs/TiO_2 hybrid film and Nb-doped TiO_2 films, and the results showed that the sensitivity of former was four times higher than that of latter, as shown in Figure 16. The outstanding sensing performance of CNTs/TiO_2 hybrid films arose from their very large surface area because of the central hollow cores and outside walls of CNTs. Luca and coworkers [149] have developed a room temperature sensor using Pt/TiO_2/MWCNTs composites. The results showed that increased resistance in response to H_2 possibly indicated a p-type conduction mechanism of the composite sensing material. Lee et al. [151] have demonstrated that the MWCNTs/TiO_2 xerogel composites film possessed better sensing performance. Compared with pure TiO_2 xerogel, the nanocomposites displayed improved sensitivity (15.8), and lower response/recovery times (4/16 s), as shown in Figure 17. The improved sensing properties could be attributed to the increased surface-to-volume area and enhanced conductivity which were benefit from the p-n heterojunction formed at the interface of MWCNTs and TiO_2. This result could also be confirmed by Kim et al. [152] who prepared a MWCNTs-modified direct-patternable TiO_2 thin film based CO gas sensor. It was found that the incorporation of MWCNTs could induce increase of surface morphology and roughness and thus resulted in promoted sensing performance.

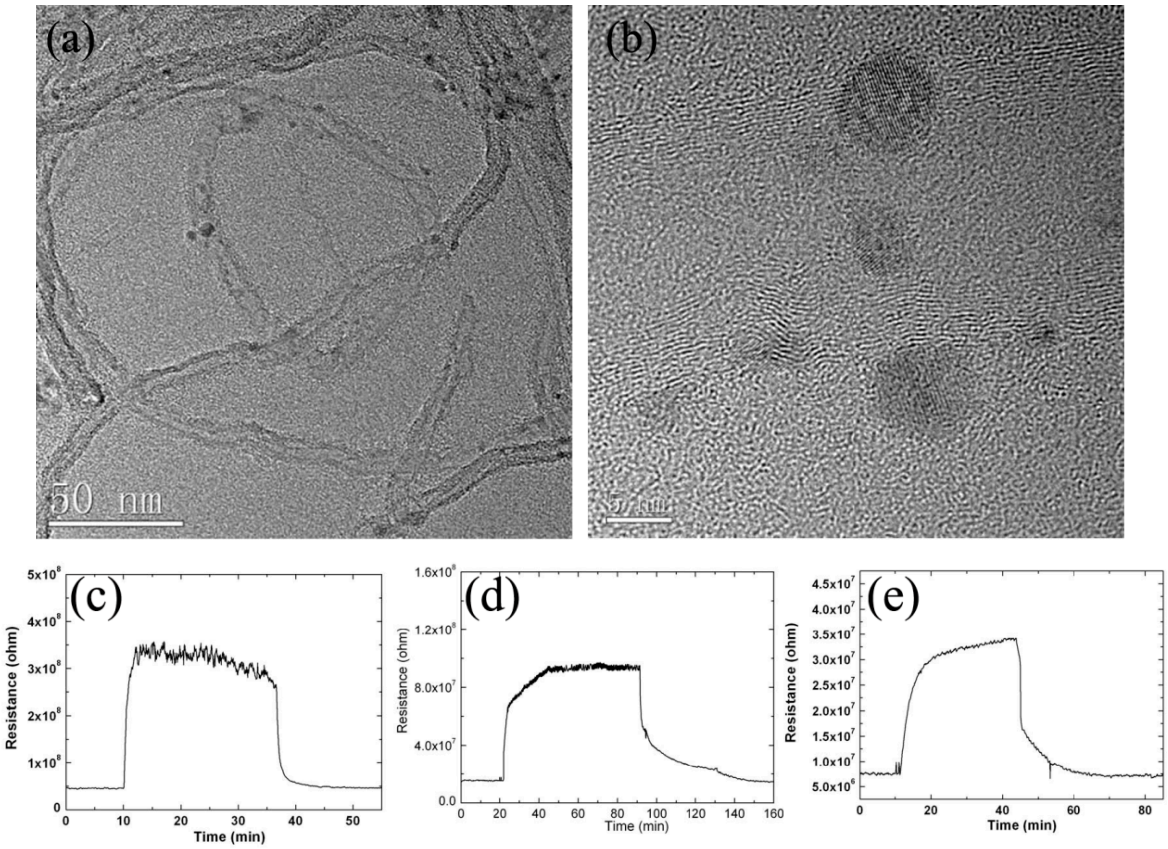

Figure 16. (**a**,**b**) HRTEM images of CNT/TiO_2 nanocmposites; (**c**–**e**) Response to 10 ppm of O_2 in CO_2 flow at 450 °C for (**a**) a TiO_2/MWCNT sensor annealed at 500 °C; (**b**) a TiO_2/MWCNT sensor annealed at 600 °C; and (**c**) a Nb-doped TiO_2/MWCNT sensor annealed at 500 °C [154]. Copyright 2008 Institute of Physics.

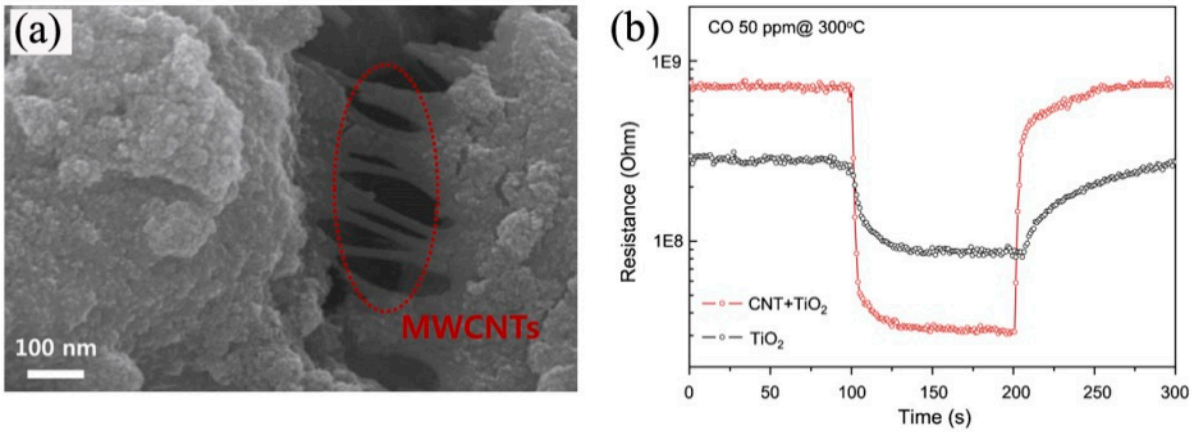

Figure 17. (**a**) SEM image of MWCNTs/TiO_2 xerogel film; (**b**) CO sensing properties of pure TiO_2 xerogel film and MWCNTs/TiO_2 xerogel film to 50 ppm CO at 350 °C [151]. Copyright 2013 Elsevier.

3.3. Organic/Inorgnic Nanoheterostructures

Nowadays, more and more requirements for gas sensors applied in the safety control and environmental monitoring have been put forward. In these efforts, designing and manufacturing suitable and efficient sensing materials is an important factor in obtaining highly efficient sensors [156]. In recent years, conductive polymers were considered a promising sensing element because of the

significant changes in electrical and optical properties of such materials exposed in different gas atmospheres. In particular, the simple preparation and high sensing performance at room temperature of these polymers make them more acceptable for applications in many fields [157].

Conducting polymer-based nanocomposites composed of metal oxides nanomaterials and conducting polymers have been well developed, and the corresponding sensors exhibit great potential in probing various hazardous gases [91] due to their enhanced sensing properties, such as fast and reversible responses to target gases at room temperature [92], and more noticeably, that defined organic material modified semiconductor sensors exhibit outstanding sensing selectivity to a single gas species because of their exclusive chemical and electronic conditions [6,158–160]. Particularly, organic-functionalized TiO_2 nanoheterostructures also exhibit significantly improved characteristics in gas sensing compared with pure TiO_2 nanomaterials [83,91,94,161,162] and thus have been investigated by several research groups, as shown in Table 3.

Till now, a number of literatures proposed the sensing mechanism of polymer/TiO_2 nanoheterostructures. One of generally accepted factor is that the nanostructures of the heterostructures are beneficial to the high sensing properties, which mainly result from their large specific surface areas and much more active sites for the adsorption and interactions with the gases [163–165]. What is more, the formation of heterojunction at the interface between TiO_2 and polymers is usually regarded as a main factor for the ultrahigh sensitivity of the nanoheterostructures [83]. At the heterostructure interface, the electrons will transfer from the material with higher Fermi level to another with lower Fermi level, while the holes will transfer rightabout until the Fermi levels is equalized. In this process, electron depletion layer, an efficient current switch, will form at the interface of the heterostructures, thus leading to high gas sensitivity [166–168].

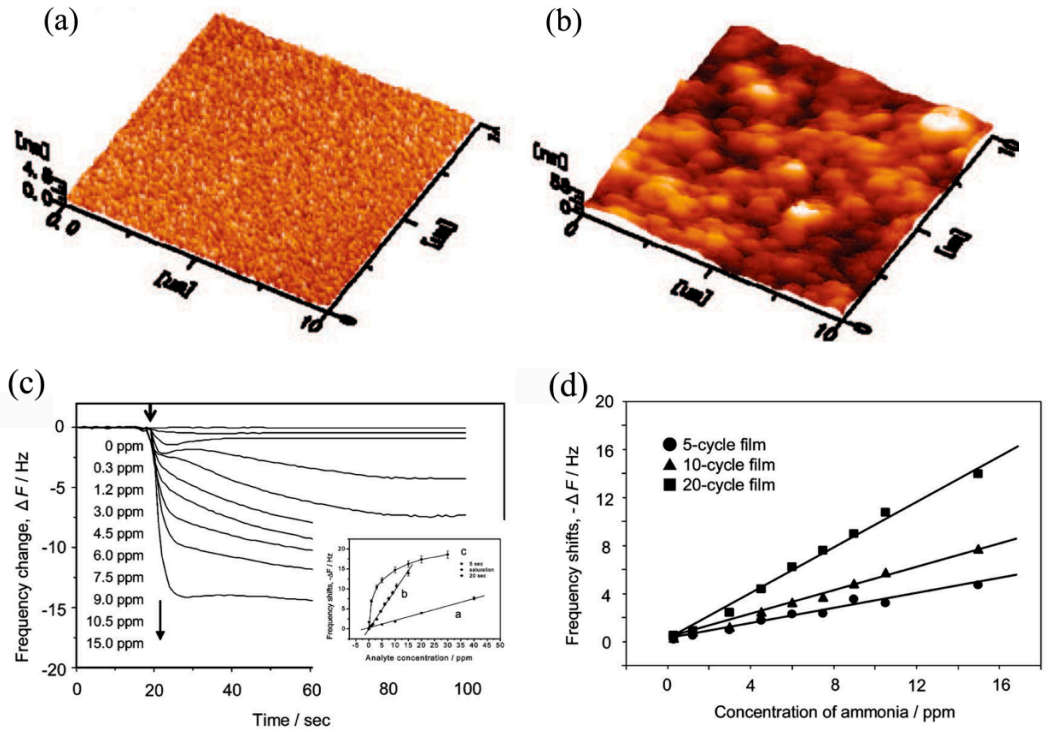

Figure 18. (**a**,**b**) Atomic force microscope (AFM) images of the surface morphology of PAA25 (**a**) and PAA400 (**b**) deposited on TiO_2 gel-immobilized mica; (**c**) Dynamic responses of the quartz crystal microbalance (QCM) electrode coated with a $(TiO_2/PAA400)_{20}$ film to ammonia at different concentrations. The inset shows a comparison of the calibration curves with data taken at different times; (**d**) Calibration curves for $(TiO_2/PAA)_n$ (n = 5, 10, and 20) films [94]. Copyright 2010 American Chemical Society.

Table 3. Summary of the gas sensing properties of TiO_2-based organic/inorganic nanoheterostructure sensors.

TiO_2-Based Nanoheterostructures	Fabrication Method	Size	Detection Gas	Detection Range	Response				Ref.
					Operation Temperature (°C)	Sensitivity	Response/ Recovery Time	Concentration	
TiO_2/PPy nanocomposites	in situ chemical polymerization	33–67 nm	NH_3	20–140 ppm	RT	$(\Delta R/R_a) \times 100\%$: 7.95%	19/85 s	141 ppm	[88]
PPy-coated TiO_2/ZnO nanofibers	electrospinning + chemical deposition	TiO_2/ZnO core diameter: 100 nm; PPy shell thickness: 7 nm	NH_3	0.5–450 ppm	RT	$\Delta R/R_a$: 0.35		450 ppm	[118]
PPy/TiO_2 nanocomposites	layer by layer self-assembly technology.		NH_3	10–1600 ppm	RT	frequency shift (ΔF): 50 Hz	~100/200 s	10 ppm	[165]
PPy/TiO_2	in situ polymerization		NH_3	20–500 ppm	RT	$\Delta R/R_a$: 0.13		100 ppm	[169]
PANi/TiO_2 nanofibers	electrospinning	diameter: 600 nm	NH_3	>50 ppt	RT	ΔR/Ra: 0.018	<10/10 s	200 ppt	[49]
PANi/TiO_2 thin film heterojunction	chemical polymerization + sol-gel		NH_3	20–100 ppm	RT	$(\Delta R/R_a) \times 100\%$: ~11%	41/- s	100 ppm	[74]
polyaniline/TiO_2 nanorods heterostructure	hydrothermal method		NH_3	5–100 ppm	RT	$(R_g/R_a) \times 100\%$: 610%	40/60 s	100 ppm	[167]
cellulose/TiO_2/PANi composite nanofibers	electrospinning		NH_3	10–250 ppm	RT	$\Delta R/R_a$: 0.584		10 ppm	[168]
TiO_2-PANi/PA6 nanofibers	electrospinning + sputtering		NH_3	50–250 ppm	RT	$\Delta R/R_a$: 18.3	<50/50 s	250 ppm	[170]
PANi/TiO_2 nanocomposite thin film	in situ self-assembly technique	diameter: 90 nm	NH_3	20–140 ppm	RT	$\Delta R/R_a$: 0.3	2–3/~60 s	1 ppm	[88]
CSA/PANi/TiO_2 thin film	sol-gel		NH_3	20–100 ppm	RT	$\Delta R/R_a$: 0.75	49/413 s	100 ppm	[171]
TiO_2–PANi nanocomposite thin film	spin coating	~20 nm	CO_2	53–1000 ppm	RT	R_g/R_a: 53	9.2/5.7 min	1000 ppm	[164]
PANi doped TiO_2 nanocomposite thin film	spin coating	21 nm	LPG		RT	R_g/R_a: 2.37	2.6/2.4 min	2000 ppm	[164]
TiO_2/PPy/poly 3-[(methacryoylamino) propyl trimethylammonium chloride] (PMAPTAC) nanocomposite thin film	in situ photopolymerization		humidity	13–90% RH	RT	log Z: ~6	30/45 s	60%	[172]
TiO_2/PPy nanocomposite film	in situ photopolymerization		humidity	30–84% RH	RT	log Z: ~5.5	40/20 s	30%	[173]

Polyacrylic acid (PAA) is one of the appropriate choices for probing NH_3 gas because the free carboxylic functional groups present on the PAA surface possess high sensitivity and selectivity to NH_3 molecules [174]. The incorporation of PAA and metal oxide nanomaterials may solve the long recovery time at higher NH_3 concentration (>1 ppm) and undesired sensitivity to humidity of the existing inorganic semiconductor sensors [175]. For instance, Lee and coworkers [94] have demonstrated that TiO_2/PAA-based amine gas sensors exhibited fast and stable response in a wide relative humidity range of 30%–70%, furthermore, a good linear response was also observed in the NH_3 concentration range between 0.3 ppm and 15 ppm, as shown in Figure 18. One of possible reasons for the decreased influence of humidity on gas sensitivity was that the presence of the TiO_2 would suppress the mobility of PAA, therefore the influence of water molecules on the sensing response would be reduced. As another very interesting conducting polymer, polypyrrole (PPy) has been widely investigated due to its relatively good environmental stability and easily controlled surface carrier properties adjusted by altering the dopant species in PPy during the synthetic process [169]. Accordingly, a number of researchers have attempted to enhance the gas sensing performance of TiO_2 by introducing PPy to form organic/inorgnic nanoheterostructures. For example, Bulakhe and coworkers [83] have prepared a PPy/TiO_2 heterojunction-based liquefied petroleum gas (LPG) sensor which could operate at room temperature. The maximum sensing sensitivity of 55% to 1040 ppm LPG was observed, as shown in Figure 19. Compared with other room temperature LPG sensors, the PPy/TiO_2 heterojunction-based sensor could work at low LPG concentrations and showed promoted response/recovery times (112/131 s), indicating the PPy/TiO_2 heterojunction was a promising choice for a room temperature LPG sensor. Furthermore, Tai et al. [88] have investigated the NH_3 sensing performance of TiO_2/PPy nanocomposite ultrathin films. The results revealed that the TiO_2/PPy ultrathin film presented outstanding sensing performance, such as shorter response/recovery time comparing with pure PPy thin film based sensor. Additionally, in the work of Wu et al. [169], the PPy/TiO_2 composite thin film based sensor displayed much lower detection limit of 2 ppm to NH_3 gas. The improvement of sensing performance of PPy/TiO_2 heterostructures is mainly attributed to the formation of p-n junctions at the interface between TiO_2 and organic PPy.

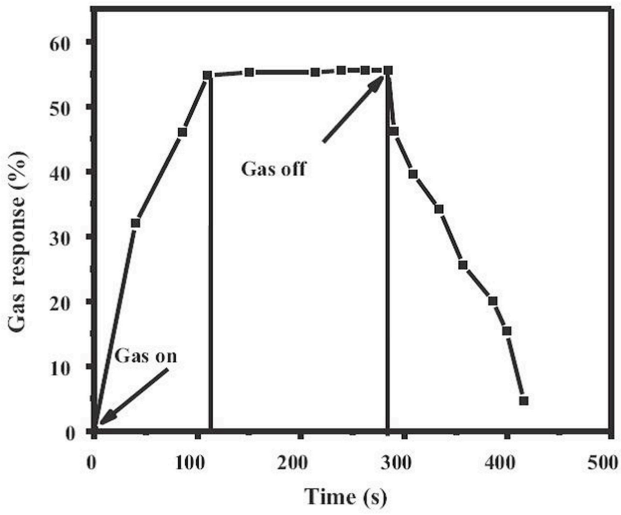

Figure 19. Gas response of a PPy/TiO_2 heterojunction at a fixed voltage of +0.6 V at concentration of 1040 ppm of LPG [83]. Copyright 2013 Elsevier.

Moreover, polyaniline (PANi) has attracted much attention in commercial applications due to its excellent environment stability, novel photoelectrical and electrical characteristics, and easy fabrication [170]. It has been demonstrated that combining TiO_2 with PANi can enhance the sensitivity, selectivity, and stability of the resulting sensors [88]. For example, Gong et al. [49] have reported an

ultrasensitive NH_3 gas sensor based on PANi/TiO_2 fibers p-n heterojunctions, it was found that the p-n heterojunctions could act as electronic transmission switches when NH_3 gas was absorbed by PANi, thus resulting in the enhancement of sensing properties. Similarly, using TiO_2 nanoparticles modified PANi fibers as sensor, a fast response of 2–3 s and a low detection limit of 1 ppm at room temperature were obtained by Tai et al. [88]. Additionally, Pawar et al. [74] have also investigated the sensing performance of nanostructured PANi/TiO_2 films synthesized via a spin-coating method on glass substrates, the results revealed that the nanocomposites film exhibited much enhanced sensing performance, such as higher sensitivity and lower respons/recover time toward NH_3 at room temperature, as shown in Figure 20.

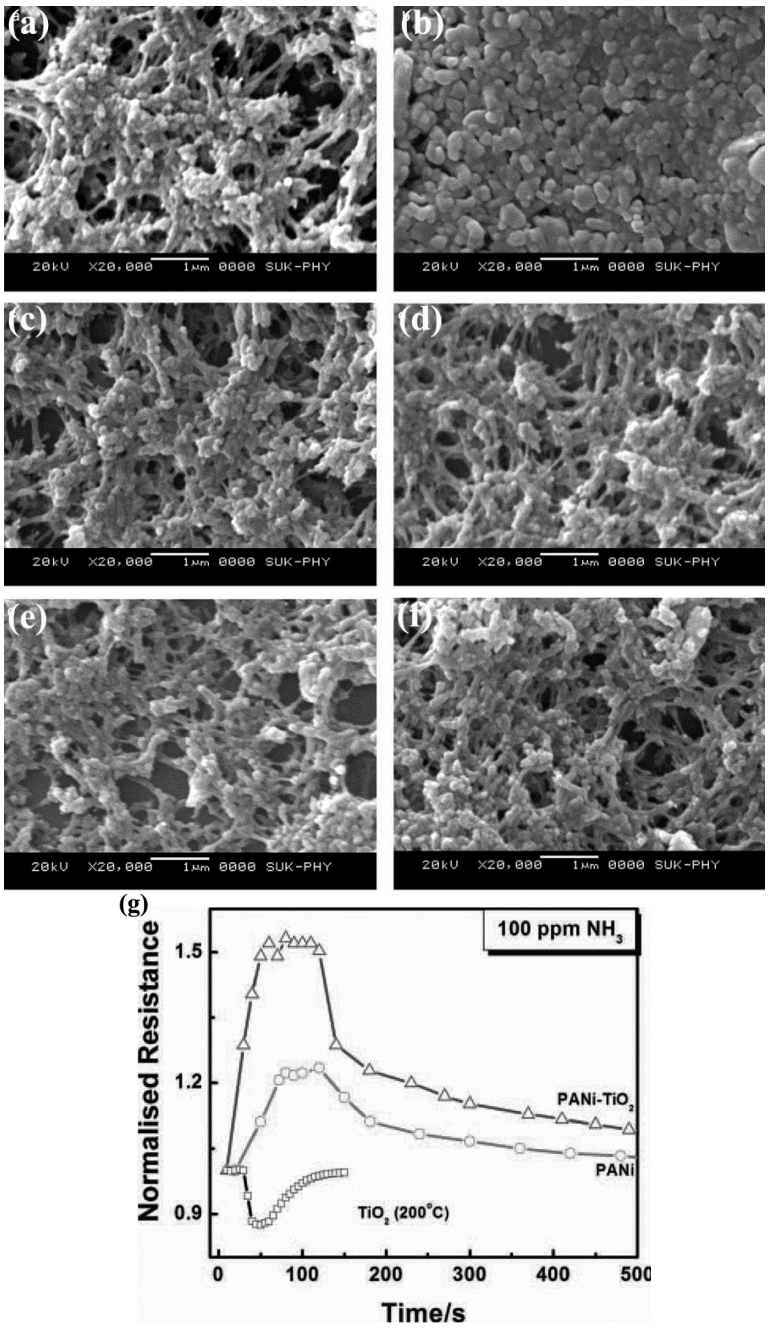

Figure 20. (a–f) SEM images of PANi (a); TiO_2 (b); and PANi–TiO_2 (20–50 wt %) films (c–f); (g) Response of the pure TiO_2, pure PANi, and nanocomposite of the PANi-TiO_2 film toward 100 ppm NH_3 gas at room temperature [74]. Copyright 2012 Wiley.

4. Conclusions

In the last few decades, continuous breakthroughs in the fabrication, modification and application of TiO_2-based gas sensors have been reported. In this review, we describe the universal tactics and new progress in the preparation of TiO_2-based nanoheterostructures for exhaust gases detecting. We focus on then synthetic methods and sensing performances of TiO_2-based nanoheterostructures, including semiconductor/semiconductor nanoheterostructures, noble metal/semiconductor nanoheterostructures, carbon-group-materials/semiconductor nanoheterostructures, and organic/inorganic nanoheterostructures, which are summarized as follows:

(1) Coupling TiO_2 by with other semiconducting materials to form heterostructures could result in enhanced sensitivity and selectivity, faster response/recovery times, and/or lower operational temperatures than pure TiO_2. The enhanced sensing properties could be related to the heterojunctions formed at the interface between two semiconductors, the synergetic effect and catalytic effect. Additionally, the influence of the nanoheterostructures' morphology on sensing performance should also be taken into account, where the gas sensitivity and the response/recovery time affected by gas absorption and gas diffusion can be promoted by the specific surface area and the special morphology of structures. As compared with other types of nanoheterostructure-based sensors, the minimization of detectable levels of the semiconductor/semiconductor nanoheterostructure-based sensors might not bear comparison with the carbon-group-materials/semiconductor nanoheterostructures, and their operation temperatures might be higher than that of noble metal/semiconductor nanoheterostructures and organic/inorganic nanoheterostructures, however, their most excellent stability make the semiconductor/semiconductor nanoheterostructures more acceptable when applied in many fields.

(2) Combining carbon-group-materials with TiO_2 is considered an efficient way to improve the gas sensing performance of TiO_2. It has been demonstrated that the absorptivity, conductivity, and/or electrochemical reactions of some small gas molecules with carbon/TiO_2 nano- heterostructures could be promoted, thus the nanoheterostructures can display remarkably improved sensing performance. Remarkably, carbon-group-material/semiconductor nano- heterostructure-based sensors display the most outstanding minimum detectable levels as compared with other nanoheterostructures, which could be attributed to their large surface area and the high electrical conductivity of the carbon-group-materials.

(3) Conducting polymer-functionalized TiO_2 nanoheterostructures have also been demonstrated to be some of most promising materials for gas detection. These nanoheterostructures possess fast and reversible responses at room temperature due to the formation of organic/inorganic heterojunctions. It is noticeable that defined organic material modified semiconductor sensors exhibit outstanding sensing selectivity to a single gas species because of their exclusive chemical and electronic conditions. As a type of typical room temperature sensor, the controllable sensing selectivity of organic/inorganic nanoheterostructures is an outstanding characteristic that other types of nanoheterostructures do not possess.

In summary, much progress has been achieved in investigation of TiO_2-based nanoheterostructured sensors, and they are widely applicable in the detection of various gases such as H_2, CO, NH_3, H_2O, VOCs, etc. However, there are still some challenges in designing high-performance nanoheterostructured gas sensors. First, although the TiO_2-based nano- heterostructured gas sensors can respond to various gases based on the resulting resistance changes, a single sensor cannot discriminate different analytes, and the response is susceptible to other gases. Thus, most current studies are focused on the quantitative analysis of target gases using only simple matrices rather than complex matrices and actual samples. To meet the needs of practical applications, one possible solution is combing multiple sensors in a multimodal module sensor system, which can display distinctive response patterns across the array in probing different actual samples. Second, the understanding to

the electrons transport and response on the interfaces of nanoheterostructures is not detailed enough, which is critical for the design and optimization of highly efficient sensors. Therefore it is necessary to further elucidate the dynamic behavior of electrons at the interface and surface of nanoheterostructures so that researchers can design TiO_2 based nanoheterostructures more rationally. Furthermore, although a variety of synthetic methods have been successfully used for preparing TiO_2-based nanoheterostructured sensors in the laboratory conditions, but these are far away from the large quantity industrial production. In addition, the chemical stability of TiO_2 based nanoheterostructures is still poor, which seriously hampers the performance and wide application of the sensors. Therefore, the in-depth understanding of the sensing mechanism and the establishing of general and reasonable design guidelines in TiO_2 based nanoheterostructured sensors are significant to achieve substantial breakthroughs in the practical application of the sensors.

Acknowledgments: We greatly acknowledge financial support from the Foundation of the Center for Compression Science (CCS) Project of China Academy of Engineering Physics (Grant No. YK2015-0602001).

Author Contributions: Y.W. and L.L. conducted all literatures referring works. Y.W. and T.W. wrote the main manuscript text. C.M. and W.Z. involved in discussion of gas sensing mechanism. Y.Z. and L.L. reviewed the manuscript.

Conflicts of Interest: The authors declare no conflict of interest.

References

1. Docherty, C.J.; Lin, C.T.; Joyce, H.J.; Nichola, R.J.; Herz, L.M.; Li, L.J.; Johnston, M.B. Extreme sensitivity of graphene photoconductivity to environmental gases. *Nat. Commun.* **2012**, *3*, 1228. [CrossRef] [PubMed]
2. Yan, Y.; Wladyka, C.; Fujii, J.; Sockanathan, S. Prdx4 is a compartment-specific H_2O_2 sensor that regulates neurogenesis by controlling surface expression of GDE2. *Nat. Commun.* **2015**, *6*, 7006. [CrossRef]
3. Lehner, P.; Staudinger, C.; Borisov, S.M.; Klimant, I. Ultra-sensitive optical oxygen sensors for characterization of nearly anoxic systems. *Nat. Commun.* **2014**, *5*, 4460. [CrossRef] [PubMed]
4. Ma, J.; Mei, L.; Chen, Y.; Li, Q.; Wang, T.; Xu, Z.; Duan, X.; Zheng, W. α-Fe_2O_3 nanochains: Ammonium acetate-based ionothermal synthesis and ultrasensitive sensors for low-ppm-level H_2S gas. *Nanoscale* **2013**, *5*, 895–898. [CrossRef] [PubMed]
5. Xu, S.; Gao, J.; Wang, L.; Kan, K.; Xie, Y.; Shen, P.; Li, L.; Shi, K. Role of the heterojunctions in In_2O_3-composite SnO_2 nanorod sensors and their remarkable gas-sensing performance for NO_x at room temperature. *Nanoscale* **2015**, *7*, 14643–14651. [CrossRef] [PubMed]
6. Hoffmann, M.W.G.; Prades, J.D.; Mayrhofer, L.; Hernandez-Ramirez, F.; Järvi, T.T.; Moseler, M.; Waag, A.; Shen, H. Highly selective SAM-nanowire hybrid NO_2 sensor: Insight into charge transfer dynamics and alignment of frontier molecular orbitals. *Adv. Funct. Mater.* **2014**, *24*, 595–602. [CrossRef]
7. Leite, E.R.; Weber, I.T.; Longo, E.; Varela, J.A. A new method to control particle size and particle size distribution of SnO_2 nanoparticles for gas sensor applications. *Adv. Mater.* **2000**, *12*, 965–968. [CrossRef]
8. Liu, J.; Wang, X.; Peng, Q.; Li, Y. Vanadium pentoxide nanobelts: Highly selective and stable ethanol sensor materials. *Adv. Mater.* **2005**, *17*, 764–767. [CrossRef]
9. Izu, N.; Hagen, G.; Schönauer, D.; Röder-Roith, U.; Moos, R. Application of $V_2O_5/WO_3/TiO_2$ for Resistive-Type SO_2 Sensors. *Sensors* **2011**, *11*, 2982–2991. [CrossRef] [PubMed]
10. Weppner, W. Solid-state electrochemical gas sensor. *Sens. Actuators* **1987**, *12*, 107–119. [CrossRef]
11. Miura, N.; Nakatou, M.; Zhuiykov, S. Impedancemetric gas sensor based on zirconia solid electrolyte and oxide sensing electrode for detecting total NO_x at high temperature. *Sens. Actuators B Chem.* **2003**, *93*, 221–228. [CrossRef]
12. Kulkarni, G.S.; Reddy, K.; Zhong, Z.; Fan, X. Graphene nanoelectronic heterodyne sensor for rapid and sensitive vapour detection. *Nat. Commun.* **2014**, *5*, 4376. [CrossRef]
13. Borini, S.; White, R.; Wei, D.; Astley, M.; Haque, S.; Spigone, E.; Harris, N.; Kivioja, J.; Ryhanen, T. Ultrafast Graphene Oxide Humidity Sensors. *ACS Nano* **2013**, *7*, 11166–11173. [CrossRef] [PubMed]
14. Chen, Z.; Umar, A.; Wang, S.; Wang, Y.; Tian, T.; Shang, Y.; Fan, Y.; Qi, Q.; Xu, D.; Jiang, L. Supramolecular fabrication of multilevel graphene-based gas sensors with high NO_2 sensibility. *Nanoscale* **2015**, *7*, 10259–10266. [CrossRef] [PubMed]

15. Lee, J.S.; Kwon, O.S.; Park, S.J.; Park, E.Y.; You, S.A.; Yoon, H.; Jang, J. Fabrication of ultrafine metal-oxide-decorated carbon nanofibers for DMMP sensor application. *ACS Nano* **2011**, *5*, 7992–8001. [CrossRef] [PubMed]
16. Gurlo, A. Nanosensors: Towards morphological control of gas sensing activity. SnO_2, In_2O_3, ZnO and WO_3 case studies. *Nanoscale* **2011**, *3*, 154–165. [CrossRef] [PubMed]
17. Seiyama, T.; Kato, A.; Fujiishi, K.; Nagatani, M. A new detector for gaseous components using semiconductor thin film. *Anal. Chem.* **1962**, *34*, 1502–1503. [CrossRef]
18. Muhr, H.J.; Krumeich, F.; Schönholzer, U.P.; Bieri, F.; Niederberger, M.; Gauckler, L.J.; Nesper, R. Vanadium oxide nanotubes-a new flexible vanadate nanophase. *Adv. Mater.* **2000**, *12*, 231–234. [CrossRef]
19. Shi, L.; Naik, A.J.T.; Goodall, J.B.M.; Tighe, C.; Gruar, R.; Binions, R.; Parkin, I.; Darr, J. Highly sensitive ZnO nanorod- and nanoprism-based NO_2 gas sensors: Size and shape control using a continuous hydrothermal pilot plant. *Langmuir* **2013**, *29*, 10603–10609. [CrossRef] [PubMed]
20. Fujishima, A.; Honda, K. Electrochemical photolysis of water at a semiconductor electrode. *Nature* **1972**, *238*, 37–38. [CrossRef] [PubMed]
21. Lin, J.; Heo, Y.U.; Nattestad, A.; Sun, Z.; Wang, L.; Kim, J.H.; Dou, S.X. 3D hierarchical rutile TiO_2 and metal-free organic sensitizer producing dye-sensitized solar cells 8.6% conversion efficiency. *Sci. Rep.* **2014**, *4*, 5769. [CrossRef] [PubMed]
22. Chen, X.; Liu, L.; Peter, Y.Y.; Mao, S.S. Increasing solar absorption for photocatalysis with black hydrogenated titanium dioxide nanocrystals. *Science* **2011**, *331*, 746–750. [CrossRef] [PubMed]
23. Paramasivam, I.; Jha, H.; Liu, N.; Schmuki, P. A review of photocatalysis using self-organized TiO_2 nanotubes and other ordered oxide nanostructures. *Small* **2012**, *8*, 3073–3103. [CrossRef] [PubMed]
24. Zarifi, M.H.; Farsinezhad, S.; Abdolrazzaghi, M.; Daneshmand, M.; Shankar, K. Selective microwave sensors exploiting the interaction of analytes with trap states in TiO_2 nanotube arrays. *Nanoscale* **2016**, *8*, 7466–7473. [CrossRef] [PubMed]
25. Si, P.; Ding, S.; Yuan, J.; Lou, X.W.; Kim, D.H. Hierarchically structured one-dimensional TiO_2 for protein immobilization, direct electrochemistry, and mediator-free glucose sensing. *ACS Nano* **2011**, *5*, 7617–7626. [CrossRef] [PubMed]
26. Bao, S.J.; Li, C.M.; Zang, J.F.; Cui, X.Q.; Qiao, Y.; Guo, J. New nanostructured TiO_2 for direct electrochemistry and glucose sensor applications. *Adv. Funct. Mater.* **2008**, *18*, 591–599. [CrossRef]
27. Wang, C.; Yin, L.; Zhang, L.; Qi, Y.; Lun, N.; Liu, N. Large scale synthesis and gas-sensing properties of anatase TiO_2 three-dimensional hierarchical nanostructures. *Langmuir* **2010**, *26*, 12841–12848. [CrossRef] [PubMed]
28. Kim, I.D.; Rothschild, A.; Lee, B.H.; Kim, D.Y.; Jo, S.M.; Tuller, H.L. Ultrasensitive chemiresistors based on electrospun TiO_2 nanofibers. *Nano Lett.* **2006**, *6*, 2009–2013. [CrossRef] [PubMed]
29. Kimura, M.; Sakai, R.; Sato, S.; Fukawa, T.; Ikehara, T.; Maeda, R.; Mihara, T. Sensing of vaporous organic compounds by TiO_2 porous films covered with polythiophene layers. *Adv. Funct. Mater.* **2012**, *22*, 469–476. [CrossRef]
30. Wang, Y.; Du, G.; Liu, H.; Liu, D.; Qin, S.; Wang, N.; Hu, C.; Tao, X.; Jiao, J.; Wang, J.; et al. Nanostructured sheets of Ti-O nanobelts for gas sensing and antibacterial applications. *Adv. Funct. Mater.* **2008**, *18*, 1131–1137. [CrossRef]
31. Linsebigler, A.L.; Lu, G.; Yates, J.T., Jr. Photocatalysis on TiO_2 surfaces: Principles, mechanisms, and selected results. *Chem. Rev.* **1995**, *95*, 735–758. [CrossRef]
32. Wunderlich, W.; Oekermann, T.; Miao, L.; Hue, N.T.; Tanemura, S.; Tanemura, M. Electronic properties of Nano-porous TiO_2- and ZnO-thin films- comparison of simulations and experiments. *J. Ceram. Proc. Res.* **2004**, *5*, 343–354.
33. Dai, J.; Yang, J.; Wang, X.H.; Zhang, L.; Li, Y.J. Enhanced visible-light photocatalytic activity for selective oxidation of amines into imines over TiO_2(B)/anatase mixed-phase nanowires. *Appl. Surf. Sci.* **2015**, *349*, 343–352. [CrossRef]
34. Yang, D.; Liu, H.; Zheng, Z.; Yuan, Y.; Zhao, J.; Waclawik, E.R.; Ke, X.; Zhu, H. An efficient photocatalyst structure: TiO_2(B) nanofibers with a shell of anatase nanocrystals. *J. Am. Chem. Soc.* **2009**, *131*, 17885–17893. [CrossRef] [PubMed]

35. Zhang, Y.; Jiang, Z.; Huang, J.; Lim, L.Y.; Li, W.; Deng, J.; Gong, D.; Tang, Y.; Lai, Y.; Chen, Z. Titanate and titania nanostructured materials for environmental and energy applications: A review. *RSC Adv.* **2015**, *5*, 79479–79510. [CrossRef]
36. Muscat, J.; Swamy, V.; Harrison, N.M. First-principles calculations of the phase stability of TiO_2. *Phys. Rev. B* **2002**, *65*, 224112. [CrossRef]
37. Altomare, M.; Dozzi, M.V.; Chiarello, G.L.; Di Paola, A.; Palmisano, L.; Selli, E. High activity of brookite TiO_2 nanoparticles in the photocatalytic abatement of ammonia in water. *Catal. Today* **2015**, *252*, 184–189. [CrossRef]
38. Nisar, J.; Topalian, Z.; De Sarkar, A.; Österlund, L.; Ahuja, R. TiO_2-based gas sensor: A possible application to SO_2. *ACS Appl. Mater. Interfaces* **2013**, *5*, 8516–8522. [CrossRef] [PubMed]
39. Bai, J.; Zhou, B. Titanium dioxide nanomaterials for sensor applications. *Chem. Rev.* **2014**, *114*, 10131–10176. [CrossRef] [PubMed]
40. Zakrzewska, K. Gas sensing mechanism of TiO_2-based thin films. *Vacuum* **2004**, *74*, 335–338. [CrossRef]
41. Göpel, W.; Schierbaum, K.D. SnO_2 sensors: Current status and future prospects. *Sens. Actuators B Chem.* **1995**, *26*, 1–12. [CrossRef]
42. Williams, D.E. Semiconducting oxides as gas-sensitive resistors. *Sens. Actuators B Chem.* **1999**, *57*, 1–16. [CrossRef]
43. Galstyan, V.; Comini, E.; Faglia, G.; Sberveglieri, G. TiO_2 nanotubes: Recent advances in synthesis and gas sensing properties. *Sensors* **2013**, *13*, 14813–14838. [CrossRef] [PubMed]
44. Li, Z.; Ding, D.; Liu, Q.; Ning, C.; Wang, X. Ni-doped TiO_2 nanotubes for wide-range hydrogen sensing. *Nanoscal. Res. Lett.* **2014**, *9*, 118–126. [CrossRef] [PubMed]
45. Lü, R.; Zhou, W.; Shi, K.; Yang, Y.; Wang, L.; Pan, K.; Tian, C.; Ren, Z.; Fu, H. Alumina decorated TiO_2 nanotubes with ordered mesoporous walls as high sensitivity NO_x gas sensors at room temperature. *Nanoscale* **2013**, *5*, 8569–8576. [CrossRef] [PubMed]
46. Barreca, D.; Comini, E.; Ferrucci, A.P.; Gasparotto, A.; Maccato, C.; Maragno, C.; Sberveglieri, G.; Tondello, E. First example of ZnO-TiO_2 nanocomposites by chemical vapor deposition: Structure, morphology, composition, and gas sensing performances. *Chem. Mater.* **2007**, *19*, 5642–5649. [CrossRef]
47. Chen, X.; Mao, S.S. Titanium dioxide nanomaterials: Synthesis, properties, modifications, and applications. *Chem. Rev.* **2007**, *107*, 2891–2959. [CrossRef] [PubMed]
48. Chaudhari, G.N.; Bambole, D.R.; Bodade, A.B.; Padole, P.R. Characterization of nanosized TiO_2 based H_2S gas sensor. *J. Mater. Sci.* **2006**, *41*, 4860–4864. [CrossRef]
49. Gong, J.; Li, Y.; Hu, Z.; Zhou, Z.; Deng, Y. Ultrasensitive NH_3 gas sensor from polyaniline nanograin enchased TiO_2 fibers. *J. Phys. Chem. C* **2010**, *114*, 9970–9974. [CrossRef]
50. Zhang, J.; Strelcov, E.; Kolmakov, A. Visible light assisted gas sensing with TiO_2 nanowires. *arXiv* **2015**, *1501*, 01877.
51. Alferov, Z.I. The double heterostructure: The concept and its applications in physics, electronics, and technology (Nobel lecture). *ChemPhysChem* **2001**, *2*, 500–513. [CrossRef]
52. Layek, A.; Middya, S.; Dey, A.; Das, M.; Datta, J.; Ray, P.P. Synthesis of ZnO composited TiO_2 nanoparticle and its application in dye sensitized solar cells: A novel approach in enhancing open-circuit voltage. *Mater. Lett.* **2014**, *126*, 214–216. [CrossRef]
53. Choi, S.H.; Kang, Y.C. One-pot facile synthesis of Janus-structured SnO_2-CuO composite nanorods and their application as anode materials in Li-ion batteries. *Nanoscale* **2013**, *5*, 4662–4668. [CrossRef] [PubMed]
54. Hernández, S.; Cauda, V.; Chiodoni, A.; Dallorto, S.; Sacco, A.; Hidalgo, D.; Celasco, E.; Pirri, C.F. Optimization of 1D ZnO@TiO_2 core-shell nanostructures for enhanced photoelectrochemical water splitting under solar light illumination. *ACS Appl. Mater. Interfaces* **2014**, *6*, 12153–12167. [CrossRef] [PubMed]
55. Tada, H.; Mitsui, T.; Kiyonaga, T.; Akita, T.; Tanaka, K. All-solid-state Z-scheme in CdS-Au-TiO_2 three-component nanojunction system. *Nat. Mater.* **2006**, *5*, 782–786. [CrossRef] [PubMed]
56. Kim, J.; Kim, W.; Yong, K. CuO/ZnO heterostructured nanorods: Photochemical synthesis and the mechanism of H_2S gas sensing. *J. Phys. Chem. C* **2012**, *116*, 15682–15691. [CrossRef]
57. Deepagan, V.G.; You, D.G.; Um, W.; Ko, H.; Kwon, S.; Choi, K.Y.; Yi, G.R.; Lee, J.Y.; Lee, D.S.; Kim, K.; et al. Long-circulating Au-TiO_2 nanocomposite as a sonosensitizer for ROS-mediated eradication of cancer. *Nano Lett.* **2016**, *16*, 6257–6264. [CrossRef]

58. Leonardi, S.G.; Aloisio, D.; Donato, N.; Russo, P.A.; Ferro, M.C.; Pinna, N.; Neri, G. Amperometric sensing of H_2O using Pt–TiO_2/reduced graphene oxide nanocomposites. *ChemElectroChem* **2014**, *1*, 617–624. [CrossRef]
59. Pandey, N.K.; Tiwari, K.; Roy, A. ZnO-TiO_2 nanocomposite: Characterization and moisture sensing studies. *Bull. Mater. Sci.* **2012**, *35*, 347–352. [CrossRef]
60. Hu, L.; Fong, C.C.; Zhang, X.; Chan, L.L.; Lam, P.K.; Chu, P.K.; Wong, K.Y.; Yang, M. Au nanoparticles decorated TiO_2 nanotube arrays as a recyclable sensor for photo-enhanced electrochemical detection of bisphenol A. *Environ. Sci. Technol.* **2016**, *50*, 4430–4438. [CrossRef] [PubMed]
61. Wang, L.; Gao, J.; Wu, B.; Kan, K.; Xu, S.; Xie, Y.; Li, L.; Shi, K. Designed synthesis of In_2O_3 beads@TiO_2-In_2O_3 composite nanofibers for high performance NO_2 sensor at room tempreture. *ACS Appl. Mater. Interfaces* **2015**, *7*, 27152–27159. [CrossRef] [PubMed]
62. Lou, Z.; Li, F.; Deng, J.; Wang, L.; Zhang, T. Branch-like hierarchical heterostructure (α-Fe_2O_3/TiO_2): A novel sensing material for trimethylamine gas sensor. *ACS Appl. Mater. Interfaces* **2013**, *5*, 12310–12316. [CrossRef] [PubMed]
63. Kong, B.; Tang, J.; Wu, Z.; Selomulya, C.; Wang, H.; Wei, J.; Wang, Y.; Zheng, G.; Zhao, D. Bio-inspired porous antenna-like nanocube/nanowire heterostructure as ultra-sensitive cellular interfaces. *NPG Asia Mater.* **2014**, *6*, e117. [CrossRef]
64. Park, S.; An, S.; Ko, H.; Lee, S.; Kim, H.W.; Lee, C. Enhanced ethanol sensing properties of TiO_2/ZnO core-shell nanorod sensors. *Appl. Phys. A* **2014**, *115*, 1223–1229. [CrossRef]
65. Wang, Y.; Wang, S.; Zhang, H.; Gao, X.; Yang, J.; Wang, L. Brookite TiO_2 decorated a-Fe_2O_3 nanoheterostructures with rod morphologies for gas sensor application. *J. Mater. Chem. A* **2014**, *2*, 7935–7943. [CrossRef]
66. Bastakoti, B.P.; Torad, N.L.; Yamauchi, Y. Polymeric micelle assembly for the direct synthesis of platinum-decorated mesoporous TiO_2 toward highly selective sensing of acetaldehyde. *ACS Appl. Mater. Interfaces* **2014**, *6*, 854–860. [CrossRef] [PubMed]
67. Da, P.; Li, W.; Lin, X.; Wang, Y.; Tang, J.; Zheng, G. Surface plasmon resonance enhanced real-time, photoelectrochemical protein sensing by Au nanoparticle-decorated TiO_2 nanowires. *Anal. Chem.* **2014**, *86*, 6633–6639. [CrossRef] [PubMed]
68. Buso, D.; Post, M.; Cantalini, C.; Mulvaney, P.; Martucci, A. Gold nanoparticle-doped TiO_2 semiconductor thin films: Gas sensing properties. *Adv. Funct. Mater.* **2008**, *18*, 3843–3849. [CrossRef]
69. Tobaldi, D.M.; Leonardi, S.G.; Pullar, R.C.; Seabra, M.P.; Neri, G.; Labrinchaa, J.A. Sensing properties and photochromism of Ag-TiO_2 nano-heterostructures. *J. Mater. Chem. A* **2016**, *4*, 9600–9613. [CrossRef]
70. Nechita, V.; Schoonman, J.; Musa, V. Ethanol and methanol sensing characteristics of Nb-doped TiO_2 porous thin films. *Phys. Status Solidi A* **2012**, *209*, 153–159. [CrossRef]
71. Barreca, D.; Carraro, G.; Comini, E.; Gasparotto, A.; Maccato, C.; Sada, C.; Sberveglieri, G.; Tondello, E. Novel synthesis and gas sensing performances of CuO-TiO_2 nanocomposites functionalized with Au nanoparticles. *J. Phys. Chem. C* **2011**, *115*, 10510–10517. [CrossRef]
72. Katoch, A.; Kim, J.H.; Kim, S.S. TiO_2/ZnO inner/outer double-layer hollow fibers for improved detection of reducing gases. *ACS Appl. Mater. Interfaces* **2014**, *6*, 21494–21499. [CrossRef] [PubMed]
73. Zhou, W.; Liu, H.; Wang, J.; Liu, D.; Du, G.; Han, S.; Lin, J.; Wang, R. Interface dominated high photocatalytic properties of electrostatic self-assembled Ag_2O/TiO_2 heterostructure. *Phys. Chem. Chem. Phys.* **2010**, *12*, 15119–15123. [CrossRef] [PubMed]
74. Pawar, S.G.; Chougule, M.A.; Sen, S.; Patil, V.B. Development of nanostructured polyaniline-titanium dioxide gas sensors for ammonia recognition. *J. Appl. Polym. Sci.* **2012**, *125*, 1418–1424. [CrossRef]
75. Ye, Z.; Tai, H.; Xie, T.; Yuan, Z.; Liu, C.; Jiang, Y. Room temperature formaldehyde sensor with enhanced performance based on reduced graphene oxide/titanium dioxide. *Sens. Actuators B Chem.* **2015**, *223*, 149–156. [CrossRef]
76. Kusior, A.; Radecka, M.; Rekas, M.; Lubecka, M.; Zakrzewska, K.; Reszka, A.; Kowalski, B.J. Sensitization of gas sensing properties in TiO_2/SnO_2 nanocomposites. *Procedia Eng.* **2012**, *47*, 1073–1076. [CrossRef]
77. Feng, C.; Xu, G.; Liu, H.; Lv, J.; Zheng, Z.; Wu, Y. Facile fabrication of Pt/graphene/TiO_2 NTAs based enzyme sensor for glucose detection. *J. Electrochem. Soc.* **2014**, *161*, B1–B8. [CrossRef]
78. Yang, Q.; Long, M.; Tan, L.; Zhang, Y.; Ouyang, J.; Liu, P.; Tang, A. Helical TiO_2 nanotube arrays modified by Cu-Cu_2O with ultrahigh sensitivity for non-enzymatic electro-oxidation of glucose. *ACS Appl. Mater. Interfaces* **2015**, *7*, 12719–12730. [CrossRef] [PubMed]

79. Huo, K.; Li, Y.; Chen, R.; Gao, B.; Peng, C.; Zhang, W.; Hu, L.; Zhang, X.; Chu, P.K. Recyclable non-enzymatic glucose sensor based on $Ni/NiTiO_3/TiO_2$ nanotube arrays. *ChemPlusChem* **2015**, *80*, 576–582. [CrossRef]
80. Liang, Y.Q.; Cui, Z.D.; Zhu, S.L.; Li, Z.Y.; Yang, X.J.; Chen, Y.J.; Ma, J.M. Design of a highly sensitive ethanol sensor using a nano-coaxial $p\text{-}Co_3O_4/n\text{-}TiO_2$ heterojunction synthesized at low temperature. *Nanoscale* **2013**, *5*, 10916–10926. [CrossRef] [PubMed]
81. Ding, L.; Ma, C.; Li, L.; Zhang, L.; Yu, J. A photoelectrochemical sensor for hydrogen sulfide in cancer cells based on the covalently and in situ grafting of CdS nanoparticles onto TiO_2 nanotubes. *J. Electroanal. Chem.* **2016**, *783*, 176–181. [CrossRef]
82. Park, S.; Kim, S.; Park, S.; Lee, W.I.; Lee, C. Effects of functionalization of TiO_2 nanotube array sensors with Pd nanoparticles on their selectivity. *Sensors* **2014**, *14*, 15849–15860. [CrossRef] [PubMed]
83. Bulakhe, R.N.; Patil, S.V.; Deshmukh, P.R.; Shinde, N.M.; Lokhande, C.D. Fabrication and performance of polypyrrole (Ppy)/TiO_2 heterojunction for room temperature operated LPG sensor. *Sens. Actuators B Chem.* **2013**, *181*, 417–423. [CrossRef]
84. Wang, Y.; Liu, L.; Xu, L.; Cao, X.; Li, X.; Huang, Y.; Meng, C.; Wang, Z.; Zhu, W. $Ag_2O/TiO_2/V_2O_5$ one-dimensional nanoheterostructures for superior solar light photocatalytic activity. *Nanoscale* **2014**, *6*, 6790–6797. [CrossRef] [PubMed]
85. Ashok, C.H.; Rao, K.V. Microwave-assisted synthesis of CuO/TiO_2. *J. Mater. Sci. Mater. Electron.* **2016**, *27*, 8816–8825. [CrossRef]
86. Buvailo, A.I.; Xing, Y.; Hines, J.; Dollahon, N.; Borguet, E. TiO_2/LiCl-based nanostructured thin film for humidity sensor applications. *ACS Appl. Mater. Interfaces* **2011**, *3*, 528–533. [CrossRef] [PubMed]
87. Zhu, T.; Ong, W.L.; Zhu, L.; Ho, G.W. TiO_2 fibers supported β-FeOOH nanostructures as efficient visible light photocatalyst and room temperature sensor. *Sci. Rep.* **2015**, *5*, 10601. [CrossRef]
88. Tai, H.; Jiang, Y.; Xie, G.; Yu, J.; Zhao, M. Self-assembly of TiO_2/polypyrrole nanocomposite ultrathin films and application for an NH_3 gas sensor. *Int. J. Environ. Anal. Chem.* **2007**, *87*, 539–551. [CrossRef]
89. Yue, J.; Chen, Z.; Yifeng, E.; Chen, L.; Zhang, J.; Song, Y.; Zhai, Y. Preparation TiO_2 core-shell nanospheres and application as efficiency drug detection sensor. *Nanoscal. Res. Lett.* **2014**, *9*, 465. [CrossRef] [PubMed]
90. Tahir, M.N.; André, R.; Sahoo, J.K.; Jochum, F.D.; Theato, P.; Natalio, F.; Berger, R.; Branscheid, R.; Kolbc, U.; Tremel, W. Hydrogen peroxide sensors for cellular imaging based on horse radish peroxidase reconstituted on polymer-functionalized TiO_2 nanorods. *Nanoscale* **2011**, *3*, 3907–3914. [CrossRef] [PubMed]
91. Chen, K.; Liu, M.; Zhao, G.; Shi, H.; Fan, L.; Zhao, S. Fabrication of a novel and simple microcystin-LR photoelectrochemical sensor with high sensitivity and selectivity. *Environ. Sci. Technol.* **2012**, *46*, 11955–11961. [CrossRef] [PubMed]
92. Wang, Y.; Chu, W.; Wang, S.; Li, Z.; Zeng, Y.; Yan, S.; Sun, Y. Simple synthesis and photoelectrochemical characterizations of polythiophene/Pd/TiO_2 composite microspheres. *ACS Appl. Mater. Interfaces* **2014**, *6*, 20197–20204. [CrossRef] [PubMed]
93. Epifani, M.; Díaz, R.; Force, C.; Comini, E.; Andreu, T.; Zamani, R.R.; Arbiol, J.; Siciliano, P.; Faglia, G.; Morante, J.R. Colloidal counterpart of the TiO_2-supported V_2O_5 system: A case study of oxide-on-oxide deposition by wet chemical techniques. synthesis, vanadium speciation, and gas-sensing enhancement. *J. Phys. Chem. C* **2013**, *117*, 20697–20705. [CrossRef]
94. Lee, S.W.; Takahara, N.; Korposh, S.; Yang, D.H.; Toko, K.; Kunitake, T. Nanoassembled thin film gas sensors. III. sensitive detection of amine odors using TiO_2/poly(acrylic acid) ultrathin film quartz crystal microbalance sensors. *Anal. Chem.* **2010**, *82*, 2228–2236. [CrossRef] [PubMed]
95. Wang, Y.; Liu, L.; Meng, C.; Zhou, Y.; Gao, Z.; Li, X.; Cao, X.; Xu, L.; Zhu, W. A novel ethanol gas sensor based on $TiO_2/Ag_{0.35}V_2O_5$ branched nanoheterostructures. *Sci. Rep.* **2016**, *6*, 33062. [CrossRef] [PubMed]
96. Wang, Y.; Liu, L.; Huang, Y.; Li, X.; Cao, X.; Xu, L.; Meng, C.; Wang, Z.; Zhu, W. $Ag_{0.35}V_2O_5/TiO_2$ branched nanoheterostructures:Facilef abrication and efficient visible light photocatalytic activity. *Mater. Lett.* **2014**, *128*, 358–361. [CrossRef]
97. Wang, Y.; Zhou, Y.; Meng, C.; Gao, Z.; Cao, X.; Li, X.; Xu, L.; Zhu, W.; Peng, X.; Zhang, B.; et al. A high-response ethanol gas sensor based on one-dimensional TiO_2/V_2O_5 branched nanoheterostructures. *Nanotechnology* **2016**, *27*, 425503. [CrossRef] [PubMed]
98. Wang, Y.; Zhang, J.; Liu, L.; Zhu, C.; Liu, X.; Su, Q. Visible light photocatalysis of V_2O_5/TiO_2 nanoheterostructures prepared via electrospinning. *Mater. Lett.* **2012**, *75*, 95–98. [CrossRef]

99. Wang, Y.; Liu, L.; Xu, L.; Meng, C.; Zhu, W. Ag/TiO_2 nanofiber heterostructures: Highly enhanced photocatalysts under visible light. *J. Appl. Phys.* **2013**, *113*, 174311. [CrossRef]
100. Li, Z.; Zhang, H.; Zheng, W.; Wang, W.; Huang, H.; Wang, C.; MacDiarmid, A.G.; Wei, Y. Highly sensitive and stable humidity nanosensors based on LiCl doped TiO_2 electrospun nanofibers. *J. Am. Chem. Soc.* **2008**, *130*, 5036–5037. [CrossRef] [PubMed]
101. Ding, Y.; Wang, Y.; Zhang, L.; Zhang, H.; Li, C.M.; Lei, Y. Preparation of TiO_2-Pt hybrid nanofibers and their application for sensitive hydrazine detection. *Nanoscale* **2011**, *3*, 1149–1157. [CrossRef]
102. Du, P.; Song, L.; Xiong, J.; Li, N.; Xi, Z.; Wang, L.; Jin, D.; Guo, S.; Yuan, Y. Coaxial electrospun TiO_2/ZnO core–sheath nanofibers film: Novel structure for photoanode of dye-sensitized solar cells. *Electrochim. Acta* **2012**, *78*, 392–397. [CrossRef]
103. Du, X.; Wang, Y.; Mu, Y.; Gui, L.; Wang, P.; Tang, Y. A new highly selective H_2 sensor based on TiO_2/PtO-Pt dual-layer films. *Chem. Mater.* **2002**, *14*, 3953–3957. [CrossRef]
104. Tomer, V.K.; Duhan, S. Ordered mesoporous Ag-doped TiO_2/SnO_2 nanocomposite based highly sensitive and selective VOC sensor. *J. Mater. Chem. A* **2016**, *4*, 1033–1043. [CrossRef]
105. Zeng, W.; Liu, T.; Wang, Z. Enhanced gas sensing properties by SnO_2 nanosphere functionalized TiO_2 nanobelts. *J. Mater. Chem.* **2012**, *22*, 3544–3548. [CrossRef]
106. Zhang, L.; Gao, Z.; Liu, C.; Zhang, Y.; Tu, Z.; Yang, X.; Yang, F.; Wen, Z.; Zhu, L.; Liu, R.; et al. Synthesis of TiO_2 decorated Co_3O_4 acicular nanowire arrays and their application as an ethanol sensor. *J. Mater. Chem. A* **2015**, *3*, 2794–2801. [CrossRef]
107. Zhu, C.L.; Yu, H.L.; Zhang, Y.; Wang, T.S.; Ouyang, Q.Y.; Qi, L.H.; Chen, Y.J.; Xue, X.Y. Fe_2O_3/TiO_2 tube-like nanostructures: Synthesis, structural transformation and the enhanced sensing properties. *ACS Appl. Mater. Interfaces* **2012**, *4*, 665–671. [CrossRef] [PubMed]
108. Chen, G.; Ji, S.; Li, H.; Kang, X.; Chang, S.; Wang, Y.; Yu, G.; Lu, J.; Claverie, J.; Sang, Y.; et al. High-energy faceted SnO_2-coated TiO_2 nanobelt heterostructure for near-ambient temperature-responsive ethanol sensor. *ACS Appl. Mater. Interfaces* **2015**, *7*, 24950–24956. [CrossRef] [PubMed]
109. Vaezi, M.R.; Shendy, S.K.; Ebadzadeh, T. Synthesis of TiO_2/SnO_2 core shell nanocomposite by chemical route and its gas sensing properties. *Indian J. Phys.* **2012**, *86*, 9–13. [CrossRef]
110. Deng, J.; Yu, B.; Lou, Z.; Wang, L.; Wang, R.; Zhang, T. Facile synthesis and enhanced ethanol sensing properties of the brush-like ZnO-TiO_2 heterojunctions nanofibers. *Sens. Actuators B Chem.* **2013**, *184*, 21–26. [CrossRef]
111. Lou, Z.; Deng, J.; Wang, L.; Wang, R.; Fei, T.; Zhang, T. A class of hierarchical nanostructures: ZnO surfacefunctionalized TiO_2 with enhanced sensing properties. *RSC Adv.* **2013**, *3*, 3131–3136. [CrossRef]
112. Deng, J.; Wang, L.; Lou, Z.; Zhang, T. Design of CuO-TiO_2 heterostructure nanofibers and their sensing performance. *J. Mater. Chem. A* **2014**, *2*, 9030–9034. [CrossRef]
113. Zeng, W.; Liu, T.; Wang, Z. Sensitivity improvement of TiO_2-doped SnO_2 to volatile organic compounds. *Phys. E Low-Dimens. Syst. Nanostructures* **2010**, *43*, 633–638. [CrossRef]
114. Zhao, Z.; Wang, D.; Kang, X.; Sang, Y.; Liu, H. Hierarchically assembled ZnO nanorods on TiO_2 nanobelts for high performance gas sensor. *Energy Environ. Focus* **2014**, *3*, 404–410. [CrossRef]
115. Zeng, W.; Liu, T.; Wang, Z.; Tsukimoto, S.; Saito, M.; Ikuhara, Y. Selective detection of formaldehyde gas using a Cd-doped TiO_2-SnO_2 sensor. *Sensors* **2009**, *9*, 9029–9038. [CrossRef] [PubMed]
116. Zhang, Z.; Huang, J.; Dong, B.; Yuan, Q.; Hea, Y.; Wolfbeis, O.S. Rational tailoring of $ZnSnO_3$/TiO_2 heterojunctions with bioinspired surface wettability for high-performance humidity nanosensors. *Nanoscale* **2015**, *7*, 4149–4155. [CrossRef] [PubMed]
117. Li, H.; Shi, Z.; Liu, H. Humidity sensing properties of La^{3+}/Ce^{3+}-doped TiO_2- 20 wt.% SnO_2 thin films derived from sol-gel method. *J. Rare Earth* **2010**, *28*, 123–127.
118. Wang, Y.; Jia, W.; Strout, T.; Schempf, A.; Zhang, H.; Li, B.; Cui, J.; Lei, Y. Ammonia gas sensor using polypyrrole-coated TiO_2/ZnO nanofibers. *Electroanalysis* **2009**, *21*, 1432–1438. [CrossRef]
119. Radecka, M.; Kusior, A.; Lacz, A.; Trenczek-Zajac, A.; Lyson-Sypien, B.; Zakrzewska, K. Nanocrystalline TiO_2/SnO_2 composites for gas sensors. *Therm. Anal. Calorim.* **2012**, *108*, 1079–1084. [CrossRef]
120. Waghmare, S.D.; Shinde, D.V.; Zate, M.K.; Konda, R.; Mane, R.S.; Han, S.H. Enhanced gas sensitivity in TiO_2 nanoneedles grown on upright SnO_2 nanoplates. *Scr. Mater.* **2013**, *68*, 735–738. [CrossRef]
121. Jung, J.Y.; Lee, C.S. Characteristics of the TiO_2/SnO_2 thick film semiconductor gas sensor to determine fish freshness. *J. Ind. Eng. Chem.* **2011**, *17*, 237–242. [CrossRef]

122. Comini, E.; Guidi, V.; Frigeri, C.; Riccò, I.; Sberveglieri, G. CO sensing properties of titanium and iron oxide nanosized thin films. *Sens. Actuators B Chem.* **2001**, *77*, 16–21. [CrossRef]
123. Bodade, A.B.; Bende, A.M.; Chaudhari, G.N. Synthesis and characterization of CdO-doped nanocrystalline ZnO: TiO_2-based H_2S gas sensor. *Vacuum* **2008**, *82*, 588–593. [CrossRef]
124. Park, S.; Kim, S.; Kheel, H.; Park, S.E.; Lee, C. Synthesis and hydrogen gas sensing properties of TiO_2-decorated CuO nanorods. *Bull. Korean Chem. Soc.* **2015**, *36*, 2458–2463. [CrossRef]
125. Devi, G.S.; Hyodo, T.; Shimizu, Y.; Egashira, M. Synthesis of mesoporous TiO_2-based powders and their gas-sensing properties. *Sens. Actuators B Chem.* **2002**, *87*, 122–129. [CrossRef]
126. Imawan, C.; Solzbacher, F.; Steffes, H.; Obermeier, E. TiO_x-modified NiO thin films for H_2 gas sensors: Effects of TiO_x-overlayer sputtering parameters. *Sens. Actuators B Chem.* **2000**, *68*, 184–188. [CrossRef]
127. Kim, H.S.; Jin, C.H.; Park, S.H.; Lee, C.M. Structural, luminescent, and NO_2 sensing properties of SnO_2-core/V_2O_5-shell nanorods. *J. Electroceram.* **2013**, *30*, 6–12. [CrossRef]
128. Zhuiykov, S.; Wlodarski, W.; Li, Y. Nanocrystalline V_2O_5-TiO_2 thin-films for oxygen sensing prepared by sol-gel process. *Sens. Actuators B Chem.* **2001**, *77*, 484–490. [CrossRef]
129. Trinchi, A.; Li, Y.X.; Wlodarski, W.; Kaciulis, S.; Pandolfi, L.; Viticoli, S.; Comini, E.; Sberveglieri, G. Investigation of sol–gel prepared CeO_2-TiO_2 thin films for oxygen gas sensing. *Sens. Actuators B Chem.* **2003**, *95*, 145–150. [CrossRef]
130. Lee, H.C.; Hwang, W.S. Substrate effects on the oxygen gas sensing properties of SnO_2/TiO_2 thin films. *Appl. Surf. Sci.* **2006**, *253*, 1889–1897. [CrossRef]
131. Wang, Y.; Su, Y.R.; Qiao, L.; Liu, L.X.; Su, Q.; Zhu, C.Q.; Liu, X.Q. Synthesis of one-dimensional TiO_2/V_2O_5 branched heterostructures and their visible light photocatalytic activity towards Rhodamine B. *Nanotechnology* **2011**, *22*, 225702. [CrossRef] [PubMed]
132. Zhang, Z.; Zou, X.; Xu, L.; Liao, L.; Liu, W.; Ho, J.; Xiao, X.; Jiang, C.; Li, J. Hydrogen gas sensor based on metal oxide nanoparticles decorated graphene transistor. *Nanoscale* **2015**, *7*, 10078–10084. [CrossRef] [PubMed]
133. Lee, B.Y.; Sung, M.G.; Lee, J.; Baik, K.Y.; Kwon, Y.K.; Lee, M.S.; Hong, S. Universal parameters for carbon nanotube network-based sensors: Can nanotube sensors be reproducible? *ACS Nano* **2011**, *5*, 4373–4379. [CrossRef] [PubMed]
134. Hu, N.; Wang, Y.; Chai, J.; Gao, R.; Yang, Z.; Kong, E.S.W.; Zhang, Y. Gas sensor based on p-phenylenediamine reduced graphene oxide. *Sens. Actuators B Chem.* **2012**, *163*, 107–114. [CrossRef]
135. Mu, H.; Wang, K.; Zhang, Z.; Xie, H. Formaldehyde graphene gas sensors modified by thermally evaporated tin oxides and tin compound films. *J. Phys. Chem. C* **2015**, *119*, 10102–10108. [CrossRef]
136. Yang, Y.; Tian, C.; Wang, J.; Sun, L.; Shi, K.; Zhou, W.; Fu, H. Facile synthesis of novel 3D nanoflower-like Cu_xO/multilayer graphene composites for room temperature NO_x gas sensor application. *Nanoscale* **2014**, *6*, 7369–7378. [CrossRef] [PubMed]
137. Fu, L.; Zheng, Y.H.; Fu, Z.X. Ascorbic acid amperometric sensor using a graphene-wrapped hierarchical TiO_2 nanocomposite. *Chem. Pap.* **2015**, *69*, 655–661. [CrossRef]
138. Jain, R.; Dhanjai. TiO_2-multi walled carbon nanotubes hybrid film sensor for sensing of antiprotozoal agent satranidazole in solubilzed system. *J. Electrochem. Soc.* **2013**, *160*, H474–H480. [CrossRef]
139. Trocino, S.; Donato, A.; Latino, M.; Donato, N.; Leonardi, S.G.; Neri, G. Pt-TiO_2/MWCNTs hybrid composites for monitoring low hydrogen concentrations in air. *Sensors* **2012**, *12*, 12361–12373. [CrossRef]
140. Ueda, T.; Takahashi, K.; Mitsugi, F.; Ikegami, T. Preparation of single-walled carbon nanotube/TiO_2 hybrid atmospheric gas sensor operated at ambient temperature. *Diam. Relat. Mater.* **2009**, *18*, 493–496. [CrossRef]
141. Ghadiry, M.; Gholami, M.; Lai, C.K.; Ahmad, H.; Chong, W.Y. Ultra-sensitive humidity sensor based on optical properties of graphene oxide and nano-anatase TiO_2. *PLoS ONE* **2016**, *11*, e0153949. [CrossRef] [PubMed]
142. Su, P.; Chen, F.; Wei, C. Simple one-pot polyol synthesis of Pd nanoparticles, TiO_2 microrods and reduced graphene oxide ternary composite for sensing NH_3 gas at room temperature. *Sens. Actuators B Chem.* **2017**, in press.
143. Amiri, M.T.; Ashkarran, A.A. Fabrication, characterization and enhanced sensing performance of graphene-TiO_2 gas sensor device. *J. Mater. Sci. Mater. Electron.* **2017**, *28*, 9435–9441. [CrossRef]

144. Li, X.; Zhao, Y.; Wang, X.; Wang, J.; Gaskov, A.M.; Akbar, S.A. Reduced graphene oxide (rGO) decorated TiO_2 microspheres forselective room-temperature gas sensors. *Sens. Actuators B Chem.* **2016**, *230*, 330–336. [CrossRef]
145. Tian, J.; Yang, G.; Jiang, D.; Su, F.; Zhang, Z. A hybrid material consisting of bulk-reduced TiO_2, graphene oxide and polyaniline for resistance based sensing of gaseous ammonia at room temperature. *Microchim. Acta* **2016**, *183*, 2871–2878. [CrossRef]
146. Xiang, C.; Jiang, D.; Zou, Y.; Chu, H.; Qiu, S.; Zhang, H.; Xu, F.; Sun, L.; Zheng, L. Ammonia sensor based on polypyrrole-graphene nanocomposite decorated with titania nanoparticles. *Ceram. Int.* **2015**, *41*, 6432–6438. [CrossRef]
147. Wang, Q.; Guo, X.; Cai, L.; Cao, Y.; Gan, L.; Liu, S.; Wang, Z.; Zhang, H.; Li, L. TiO_2-decorated graphenes as efficient photoswitches with high oxygen sensitivity. *Chem. Sci.* **2011**, *2*, 1860–1864. [CrossRef]
148. Sánchez, M.; Rincón, M.E. Sensor response of sol–gel multiwalled carbon nanotubes-TiO_2 composites deposited by screen-printing and dip-coating techniques. *Sens. Actuators B Chem.* **2009**, *140*, 17–23. [CrossRef]
149. Jiang, L.; Zhang, W. Electrodeposition of TiO_2 nanoparticles on multiwalled carbon nanotube arrays for hydrogen peroxide sensing. *Electroanalysis* **2009**, *21*, 988–993. [CrossRef]
150. Ampelli, C.; Spadaro, D.; Neri, G.; Donato, N.; Latino, M.; Passalacqua, R.; Perathoner, S.; Centi, G. Development of hydrogen leak sensors for fuel cell transportation. *Chem. Eng. Trans.* **2012**, *26*, 333–338.
151. Lee, J.S.; Ha, T.J.; Hong, M.H.; Park, C.S.; Park, H.H. The effect of multiwalled carbon nanotube doping on the CO gas sensitivity of TiO_2 xerogel composite film. *Appl. Surf. Sci.* **2013**, *269*, 125–128. [CrossRef]
152. Kim, H.; Hong, M.H.; Jang, H.W.; Yoon, S.J.; Park, H.H. CO gas sensing properties of direct-patternable TiO_2 thin films containing multi-wall carbon nanotubes. *Thin Solid Films* **2013**, *529*, 89–93. [CrossRef]
153. Liou, W.J.; Lin, H.M. Nanohybrid TiO_2/carbon black sensor for NO_2 gas. *China Part.* **2007**, *5*, 225–229. [CrossRef]
154. Llobet, E.; Espinosa, E.H.; Sotter, E.; Ionescu, R.; Vilanova, X.; Torres, J.; Felten, A.; Pireaux, J.J.; Ke, X.; Van Tendeloo, G.; et al. Carbon nanotube-TiO_2 hybrid films for detecting traces of O_2. *Nanotechnology* **2008**, *19*, 375501. [CrossRef]
155. Ensafi, A.A.; Karimi-Maleh, H. Determination of 6-mercaptopurine in the presence of uric acid using modified multiwall carbon nanotubes-TiO_2 as a voltammetric sensor. *Drug Test. Anal.* **2011**, *4*, 970–977. [CrossRef] [PubMed]
156. Prasad, G.K.; Radhakrishnan, T.P.; Sravan Kumar, D.; Ghanshyam Krishna, M. Ammonia sensing characteristics of thin film based on polyelectrolyte templated polyaniline. *Sens. Actuators B Chem.* **2005**, *106*, 626–631.
157. Wrenn, C. Real-time measurement of ammonia gas. *Occup. Health Saf.* **2000**, *69*, 64–67. [PubMed]
158. Prades, J.D.; Jimenez-Diaz, R.; Hernandez-Ramirez, F.; Barth, S.; Cirera, A.; Romano-Rodriguez, A.; Mathur, S.; Morante, J.R. Ultralow power consumption gas sensors based on self-heated individual nanowires. *Appl. Phys. Lett.* **2008**, *93*, 123110. [CrossRef]
159. Hernandez-Ramirez, F.; Prades, J.D.; Tarancon, A.; Barth, S.; Casals, O.; Jimenez-Diaz, R.; Pellicer, E.; Rodriguez, J.; Morante, J.R.; Juli, M.A.; et al. Insight into the role of oxygen diffusion in the sensing mechanisms of SnO_2 nanowires. *Adv. Funct. Mater.* **2008**, *18*, 2990–2994. [CrossRef]
160. Hoffmann, M.W.; Gad, A.E.; Prades, J.D.; Hernandez-Ramirez, F.; Fiz, R.; Shen, H.; Mathur, S. Solar diode sensor: Sensing mechanism and applications. *Nano Energy* **2013**, *2*, 514–522. [CrossRef]
161. Lu, B.; Liu, M.; Shi, H.; Huang, X.; Zhao, G. A novel photoelectrochemical sensor for bisphenol A with high sensitivity and selectivity based on surface molecularly imprinted polypyrrole modified TiO_2 nanotubes. *Electroanalysis* **2013**, *25*, 771–779. [CrossRef]
162. Dou, Y.; Han, J.; Wang, T.; Wei, M.; Evans, D.G.; Duan, X. Fabrication of MMO-TiO_2 one-dimensional photonic crystal and its application as a colorimetric sensor. *J. Mater. Chem.* **2012**, *22*, 14001–14007. [CrossRef]
163. Sonker, R.K.; Sabhajeet, S.R. Yadav, B.C. TiO_2-PANI nanocomposite thin film prepared by spin coating technique working as room temperature CO_2 gas sensing. *J. Mater. Sci. Mater. Electron.* **2016**, *27*, 11726–11732. [CrossRef]
164. Sonker, R.K.; Yadav, B.C.; Sabhajeet, S.R. Preparation of PANI doped TiO_2 nanocomposite thin film and its relevance as room temperature liquefied petroleum gas sensor. *J. Mater. Sci. Mater. Electron.* **2017**, in press.

165. Cui, S.; Yang, L.; Wang, J.; Wang, X. Fabrication of a sensitive gas sensor based on PPy/TiO_2 nanocomposites films by layer-by-layer self-assembly and itsapplication in food storage. *Sens. Actuators B Chem.* **2016**, *233*, 337–346. [CrossRef]
166. Chandra, R.M.; Reddy, P.S.P.; Rao, T.S.; Pammi, S.V.N.; Kumar, K.S.; Babu, V.V.; Kumar, Ch.K.; Hemalatha, K.P.J. Enhanced visible-light photocatalysis and gas sensor properties of polythiophene supported tin doped titanium nanocomposite. *J. Phys. Chem. Solids* **2017**, *105*, 99–105. [CrossRef]
167. Patil, U.V.; Ramgir, N.S.; Debnath, A.K.; Karmakar, N.; Aswal, D.K.; Kothari, D.C.; Gupta, S.K. NH_3 sensing properties polyaniline: TiO_2 nanorods heterostructure. *AIP Conf. Proc.* **2016**, *1731*, 050033.
168. Pang, Z.; Yang, Z.; Chen, Y.; Zhang, J.; Wang, Q.; Huang, F.; Wei, Q. A room temperature ammonia gas sensor based on cellulose/TiO_2/PANI composite nanofibers. *Colloids Surf. A* **2016**, *494*, 248–255. [CrossRef]
169. Wu, Y.; Xing, S.; Fu, J. Examining the use of TiO_2 to enhance the NH_3 sensitivity of polypyrrole films. *Appl. Polym. Sci.* **2010**, *118*, 3351–3356. [CrossRef]
170. Wang, Q.; Dong, X.; Pang, Z.; Du, Y.; Xia, X.; Wei, Q.; Huang, F. Ammonia sensing behaviors of TiO_2-PANI/PA6 composite nanofibers. *Sensors* **2012**, *12*, 17046–17057. [CrossRef] [PubMed]
171. Pawar, S.G.; Patil, S.L.; Chougule, M.A.; Raut, B.T.; Godase, P.R.; Mulik, R.N.; Sen, S.; Patil, V.B. New method for fabrication of CSA doped PANi-TiO_2 thin-film ammonia sensor. *IEEE Sens.* **2011**, *11*, 2980–2985. [CrossRef]
172. Su, P.G.; Wang, C.P. Flexible humidity sensor based on TiO_2 nanoparticles-polypyrrole-poly-[3-(methacrylamino) propyl] trimethyl ammonium chloride composite materials. *Sens. Actuators B Chem.* **2008**, *129*, 538–543. [CrossRef]
173. Su, P.G.; Huang, L.N. Humidity sensors based on TiO_2 nanoparticles/polypyrrole composite thin films. *Sens. Actuators B Chem.* **2007**, *123*, 501–507. [CrossRef]
174. Oprea, A.; Barsan, N.; Weimar, U. Ammonia detection mechanism with polyacrylic acid sensitive layers: Field effect transduction. *Sens. Actuators B Chem.* **2005**, *111*, 577–581. [CrossRef]
175. Huang, J.; Ichinose, I.; Toyoki Kunitake, A.; Nakao, A. Zirconia−titania nanofilm with composition gradient. *Nano Lett.* **2002**, *2*, 669–672. [CrossRef]